



THE UNIVERSITY *of* EDINBURGH

Edinburgh Research Explorer

Binuclear Cobalt Complexes of Schiff-Base Calixpyrroles and Their Roles in the Catalytic Reduction of Dioxygen

Citation for published version:

Volpe, M, Hartnett, H, Leeland, JW, Wills, K, Ogunshun, M, Duncombe, BJ, Wilson, C, Blake, AJ, McMaster, J & Love, JB 2009, 'Binuclear Cobalt Complexes of Schiff-Base Calixpyrroles and Their Roles in the Catalytic Reduction of Dioxygen' *Inorganic Chemistry*, vol. 48, no. 12, pp. 5195-5207. DOI: 10.1021/ic9001175

Digital Object Identifier (DOI):

[10.1021/ic9001175](https://doi.org/10.1021/ic9001175)

Link:

[Link to publication record in Edinburgh Research Explorer](#)

Document Version:

Peer reviewed version

Published In:

Inorganic Chemistry

Publisher Rights Statement:

Copyright © 2009 by the American Chemical Society. All rights reserved.

General rights

Copyright for the publications made accessible via the Edinburgh Research Explorer is retained by the author(s) and / or other copyright owners and it is a condition of accessing these publications that users recognise and abide by the legal requirements associated with these rights.

Take down policy

The University of Edinburgh has made every reasonable effort to ensure that Edinburgh Research Explorer content complies with UK legislation. If you believe that the public display of this file breaches copyright please contact openaccess@ed.ac.uk providing details, and we will remove access to the work immediately and investigate your claim.



This document is the Accepted Manuscript version of a Published Work that appeared in final form in *Inorganic Chemistry*, copyright © American Chemical Society after peer review and technical editing by the publisher. To access the final edited and published work see <http://dx.doi.org/10.1021/ic9001175>

Cite as:

Volpe, M., Hartnett, H., Leeland, J. W., Wills, K., Ogunshun, M., Duncombe, B. J., Wilson, C., Blake, A. J., McMaster, J., & Love, J. B. (2009). Binuclear Cobalt Complexes of Schiff-Base Calixpyrroles and Their Roles in the Catalytic Reduction of Dioxygen. *Inorganic Chemistry*, 48(12), 5195-5207.

Manuscript received: 20/01/2009; Article published: 11/05/2009

Binuclear cobalt complexes of Schiff-base calixpyrroles and their roles in the catalytic reduction of dioxygen**

Manuel Volpe,¹ Heather Hartnett,² James W. Leeland,^{1,2} Kathryn Wills,¹ Marianne Ogunshun,¹ Bridgette J. Duncombe,¹ Claire Wilson,^{2,3} Alexander J. Blake,² Jon McMaster² and Jason B. Love^{1,*}

^[1]EaStCHEM, School of Chemistry, Joseph Black Building, University of Edinburgh, West Mains Road, Edinburgh, EH9 3JJ, UK.

^[2]School of Chemistry, University of Nottingham, University Park, Nottingham NH7 2RD, UK.

^[3]Rigaku Europe, Chaucer Business Park, Watery Lane, Sevenoaks, Kent TN15 6QY, UK.

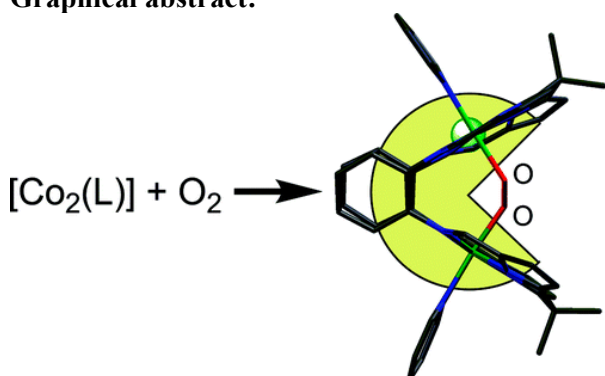
^[*]Corresponding author; e-mail: jason.love@ed.ac.uk, tel.: +44 131 6504762

^[**]We thank the Universities of Edinburgh and Nottingham for their support, the British Mass Spectrometry Society and the Nuffield Foundation for their provision of undergraduate research bursaries to KW and HH, respectively, Prof. Bill Clegg of the University of Newcastle and the EPSRC X-ray diffraction Service at the University of Southampton for the collection of X-ray data at the Synchrotron Radiation Source, Daresbury, and Dr. E. Stephen Davies at the University of Nottingham for assistance with some of the cyclic voltammetry experiments.

Supporting information:

Additional figures and tables. This material is available free of charge via the Internet at <http://pubs.acs.org>

Graphical abstract:



Synopsis:

Bimetallic cobalt Pacman complexes of octadentate Schiff-base calixpyrroles bind dioxygen as a 90:10 peroxy/superoxo mixture within the molecular cleft in a bridged Pauling mode and can act as catalysts for the reduction of dioxygen to water.

Abstract

The syntheses and characterisation of a series of binuclear cobalt complexes of the octadentate Schiff-base calixpyrrole ligand L are described. The cobalt(II) complex $[\text{Co}_2(\text{L})]$ was prepared by a transamination method and was found to adopt a wedged, Pacman geometry in the solid state and solution. Exposure of this compound to dioxygen resulted in the formation of a 90:10 mixture of the peroxo $[\text{Co}_2(\text{O}_2)(\text{L})]$ and superoxo $[\text{Co}_2(\text{O}_2)(\text{L})]^+$ complexes in which the peroxo ligand was found to bind in a Pauling mode in the binuclear cleft in pyridine and acetonitrile adducts in the solid state. The dioxygen compounds can also be prepared directly from $\text{Co}(\text{OAc})_2$ and H_4L under aerobic conditions in the presence of base. The reduction of dioxygen catalysed by this mixture of compounds was investigated using cyclic voltammetry, rotating ring disk electrochemistry, and in acidified ferrocene solutions using UV-vis spectrophotometry, and although no formation of peroxide was seen, reaction rates were slow and with limited turnover. The deactivation of the catalyst material is thought to be due to a combination of the formation of stable hydroxy-bridged binuclear complexes, *e.g.* $[\text{Co}_2(\text{OH})(\text{L})]^+$, an example of which were characterised structurally, and that the catalytic resting point, the superoxo cation, is formed by a pathway independent to the major peroxo product. Collision induced dissociation mass spectrometry experiments showed that while $[\text{Co}_2(\text{O}_2)(\text{L})]\text{H}^+$ ions readily lose a single O-atom, the resulting Co-O(H)-Co core remains resistant to further fragmentation. Furthermore, DFT calculations show that the O-O bond distance in the dioxygen complexes is not a good indicator of the degree of reduction of the O_2 unit, and provide a reduction potential of *ca.* + 0.40 V *vs.* NHE for the $[\text{Co}_2(\text{O}_2)(\text{L})]^{+/0}$ couple in dichloromethane solution.

Introduction

The oxygen reduction reaction (ORR) to water is a chemical redox reaction that is fundamental to the fuel cell technologies that underpin a low carbon, hydrogen-based economy.¹ In a polymer electrolyte fuel cell, a potential power source for zero-emission vehicles, this reaction is currently catalysed at platinum metal-based electrodes. However, the high cost of this precious metal and the high loading required for the electrode to function appropriately, the need for overpotentials to be applied, and the problems associated with electrode poisoning and degradation, necessitates the development and exploitation of new, non-precious metal catalysts to fully enable this technology.^{2,3}

The most promising class of non-precious-metal oxygen reduction catalysts are derived from iron and cobalt complexes of N-donor ligands such as porphyrins, phthalocyanines, aza-macrocycles, and also from more simple combinations of metal, nitrogen and carbon sources. While materials derived directly from these metal complexes generally have limited use as ORR catalysts, pyrolysis at temperatures between 400 and 1000 °C results in materials containing M-N_x surface species that can act as very active catalysts and that display similar characteristics to platinum.³ More recently however, it was shown that a composite of cobalt cations

and polypyrrole on a carbon support forms a cathodic electrode material that displays activity similar to platinum-based electrodes and remarkable stability.⁴ Significantly, and unlike materials derived from MN_4 complexes, no sintering of this electrode was required to provide appreciable activity. Even so, surface analysis of this material by XANES and XAFS suggests that cobalt(II) cations are present at the electrode surface and that they are stabilised by coordinative bonding to N or O.

While the most promising non-platinum electrode materials to date have been developed using high temperature sintering or supported-metal methods, many of the fundamental mechanistic aspects of dioxygen reduction catalysis have been elucidated by extensive research into molecular transition metal dioxygen complexes. In particular, binuclear cobalt compounds of cofacial diporphyrins have been shown to manage successfully the multiple proton-coupled-electron-transfer (PCET) chemistry that operates during the four-electron reduction of dioxygen to water, as opposed to the two-electron routes normally seen using mononuclear porphyrin complexes.^{5,6} This chemistry benefits from the use of prefabricated ligands, in this case cofacial diporphyrins, which control precisely the primary coordination spheres and the relative positioning of the two metals, and enables tuning of the reaction attributes through subtle modification of the ligand environment. For example, ligand modifications to form binucleating porphyrin-corrole, corrole-corrole, and porphyrin-‘Hangman’ ligands with rigid single-pillar backbones results in metal complexes that exhibit relevant PCET chemistry and that can act as ORR catalysts.^{7,8}

As an alternative approach, we,^{9,10} and Sessler and coworkers,¹¹ have shown that mono- and binuclear complexes of the Schiff-base calixpyrrole macrocycles H_4L (Chart 1) adopt rigid wedged structures that are reminiscent of those of cofacial, or Pacman, diporphyrins, albeit with much more geometrically-constrained architectures. Importantly, and in contrast to the porphyrinic analogues, these macrocyclic ligands are prepared straightforwardly in a modular manner, in high yield, and on a large scale (>30g) from inexpensive starting materials (pyrrole, ketone, aromatic diamine).

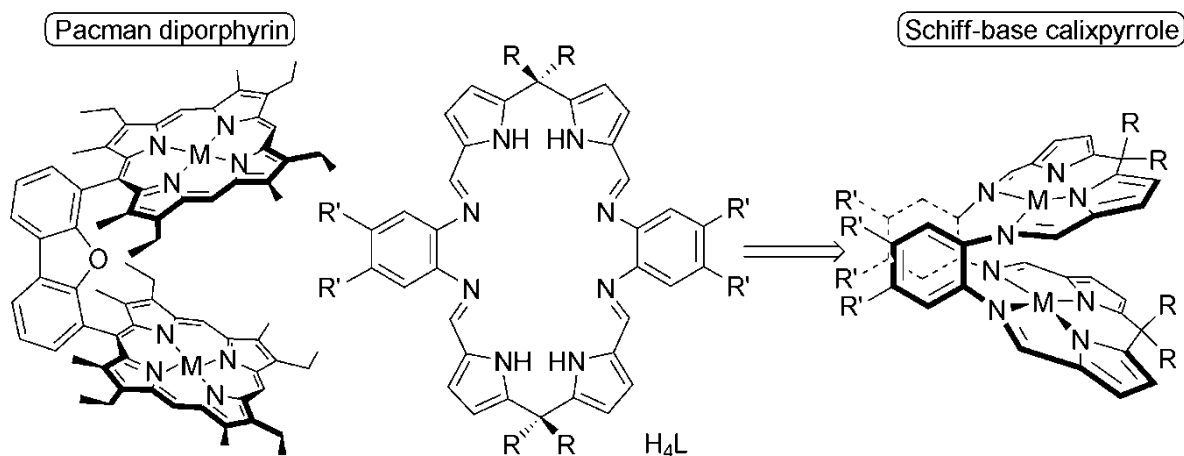


Chart 1. Comparison between Pac-man diporphyrin and Schiff-base calixpyrrole complexes

Significantly, we described in a recent communication that the binuclear cobalt complex $[\text{Co}_2(\text{L})]$ ($\text{R} = \text{Me}$, $\text{R}' = \text{H}$) reacts with dioxygen to form a 90:10 mixture of peroxo $[\text{Co}_2(\text{O}_2)(\text{L})]$ and superoxo complexes $[\text{Co}_2(\text{O}_2)(\text{L})]^+$.¹² The peroxo was found to bridge the two cobalt(III) centres in a zigzag, Pauling bonding mode in the solid state, and so provides some insight into the dioxygen reduction chemistry exhibited by related binuclear cobalt complexes of cofacial diporphyrins. In the case of the latter porphyrinic compounds, the resting state of the catalytic reduction reaction is the superoxo cation $[\text{Co}_2(\text{O}_2)(\text{diporph})]^+$ (where diporph is a cofacial, or Pacman diporphyrin ligand) in which the superoxo ligand has been shown by calculation to adopt either Griffith or Pauling bonding geometries between the two metals.^{13, 14} In this contribution, we expand on our recently communicated dioxygen chemistry of $[\text{Co}_2(\text{L})]$, in particular by assessing these materials as catalysts for dioxygen reduction, and presenting some insight into possible pitfalls in the catalytic process that operates using these catalysts.

Experimental Section

Air-sensitive metal complexation reactions were carried out using standard Schlenk line techniques or in a Vacuum Atmospheres OmniLab glovebox. The compounds H_4L and $[\text{Co}(\text{thf})\{\text{N}(\text{SiMe}_3)_2\}_2]$ were prepared using literature procedures.^{10, 15} THF and toluene were dried by passage through columns of activated alumina and collection under an inert atmosphere, while benzonitrile was dried over CaH_2 and trap-to-trap distilled. Deuteriated solvents were dried over appropriate drying agents (K: C_6D_6 , d_5 -pyridine; activated Al_2O_3 : CDCl_3), trap-to-trap distilled, and freeze-pump-thaw degassed three times before use. All other solvents and reagents were used as received. ^1H NMR spectra were recorded using a Bruker ARX250 spectrometer operating at 250.13 MHz, with residual protic impurities serving as internal standard. Electrospray mass spectra were recorded using a Thermo-Finnigan LCQ Classic ion trap mass spectrometer. Solutions of $[\text{Co}_2(\text{O}_2)(\text{L})]$ at concentrations of $18\mu\text{M}$ or $9\mu\text{M}$ were prepared in laboratory grade acetonitrile (purchased from Fischer Scientific and used without further purification) and injected at a flow rate of between 5 – 7 $\mu\text{L}/\text{min}$ into the ion trap mass spectrometer via the external, atmospheric pressure electrospray ionisation (ESI) source held at a potential of 4.5kV. The resultant ions were transferred through a heated capillary (63°C) and focussed through two octapole lenses prior to entering the quadrupole ion trap where ions are collisionally-cooled with helium buffer gas. UV/Vis spectra were recorded on a Perkin-Elmer Lambda 5 spectrophotometer and IR spectra on a Nicolet Avatar 320 FTIR spectrometer equipped with an ATR device or as Nujol mulls. Fluid solution EPR spectra were recorded at 300 K in THF using a Bruker EPX080 spectrometer and were simulated using the Bruker WINEPR SimFonia program. Magnetic susceptibilities were determined in solution using Evans' method,¹⁶ and the data corrected for the diamagnetic contribution using Pascal's constants. XPS data were recorded by Ms Emily F. Smith of the University of Nottingham on solid samples mounted on adhesive tape using a Kratos AXIS ULTRA X-ray Photoelectron Spectroscopy instrument employing a monochromated Al- K_α X-ray source ($h\nu = 1486.6\text{ eV}$) and were processed using the

CASA XPS software package (version 2.3.2). Elemental analyses were carried out by Mr. Stephen Boyer at the London Metropolitan University.

Synthesis of [Co₂(L)] and [Co₂(py)₂(L)] – Under nitrogen, a solution of [Co(thf){N(SiMe₃)₂]₂] (2.30 g, 4.96 mmol) in THF (15 mL) was added dropwise by cannula to a suspension of H₄L (1.50 g, 2.48 mmol) in THF (50 mL) at room temperature. The resulting deep red solution was stirred for 16 h, evaporated to dryness under vacuum, and extracted into hot toluene (50 mL). The hot solution was then filtered by cannula and the filtrate stored at -30° overnight. Deep red crystals of [Co₂(L)] (0.89 g, 50%), were isolated by decanting the supernatant liquors and were dried under vacuum. X-ray quality crystals of [Co₂(L)] were grown by slow cooling (-30°) a saturated toluene solution, while diffusion of Et₂O into a toluene/pyridine solution afforded black crystals of the doubly-solvated species [Co₂(py)₂(L)].

Analysis [Co₂(L)]. Found: C, 63.4; H, 4.43; N, 15.6. C₃₈H₃₂N₈Co₂ requires: C, 63.5; H, 4.49; N, 15.6 % ¹H NMR (C₆D₆): δ_H 77.4 (br.s, 4H), 39.0 (br.s, 4H), -10.7 (br.s, 4H), -26.1 (br.s, 6H), -30.4 (br.s, 10H), -45.8 (br.s, 4H). Magnetic susceptibility (C₆D₆): μ_{eff} = 3.40 μ_B; UV/Vis (THF): λ_{max} 214 (243700), 262 (64117), 270 (57270), 329 nm (ε = 81745 mol⁻¹Lcm⁻¹)

Synthesis of [Co₂(O₂)(py)₂(L)]

Method 1 - A stirred suspension of H₄L (0.200 g, 0.331 mmol) in CHCl₃ (15 mL) was treated with a solution of Co(OAc)₂·4H₂O (0.165 g, 0.662 mmol) in MeOH (ca. 1 mL) under an air atmosphere. The resultant mixture was stirred for 0.5 h at room temperature, after which the solids had dissolved, and was treated with a few drops of NEt₃. The deep brown solution was stirred for 8 h, after which the solvent was removed under vacuum. The crude material was redissolved in MeOH (50 mL) and filtered, solvent was removed from the filtrate under reduced pressure, the resulting solids were redissolved in minimal CHCl₃ and the crude pale brown solids precipitated by the addition of 100 mL of Et₂O and collected by suction filtration (0.188 g, 76%).

Analysis for [Co₂(O₂)(L)]. Found: C, 60.73; H, 4.41; N, 14.83. C₃₈H₃₂N₈Co₂O₂ requires C, 60.81; H, 4.30; N, 14.93%; IR (ATR): 1613, 1330, 1269, 1204, 1046 cm⁻¹; UV/vis (CHCl₃): λ_{max} 324 nm (ε = 29700 mol⁻¹Lcm⁻¹), 480 (6600); ESI-MS: *m/z* 735 (M⁺+1); EPR (300K): *g* 2.028, A(Co) 11.70 G.

The pyridine adduct [Co₂(O₂)(py)₂(L)] was obtained by diffusing Et₂O vapour into a MeOH/pyridine solution of [Co₂(O₂)(L)] as black columns (37%).

UV/vis (CHCl₃): λ_{max} 330 nm (ε = 26100 mol⁻¹Lcm⁻¹), 484 (5800); ESI-MS (+ve ion): *m/z* 735 (M⁺ - 2py - O); ¹H NMR (CDCl₃): δ_H 8.20 (br.s, 4H, *o/m*-py), 7.98 (s, 4H, N=CH), 7.59 (m, 2H, *p*-py), 7.21 (m, 4H, *o/m*-py), 7.12 (d, 4H, *J* = 3.8 Hz, pyrrole), 6.83 (m, 4H, aryl), 6.38 (br.s, m, 4H, aryl), 6.32 (d, 4H, *J* = 3.8 Hz, pyrrole), 1.52 (s, 6H, *meso*-CH₃), 1.21 (s, 6H, *meso*-CH₃). EPR (300K, THF): *g* 2.028, A(Co) 12.04 G, A(N) 2.00 G

Method 2 - A solution of $[\text{Co}_2(\text{L})]$ (0.150 g, 0.209 mmol) in dry CHCl_3 (25 mL) was degassed and exposed to air, resulting in an immediate dark red to dark brown colour change. Pyridine (0.5 mL) was added, and the mixture reduced in volume. The addition of Et_2O (25 mL) caused 0.085 g, 45 % of $[\text{Co}_2(\text{O}_2)(\text{py})_2(\text{L})]$ to precipitate as dark brown solids that were isolated by filtration, washed with Et_2O (2 x 5 mL) and dried under vacuum.

Analysis for $[\text{Co}_2(\text{O}_2)(\text{py})_2(\text{L})]$. Found: C, 63.5; H, 4.54; N, 15.3. $\text{C}_{48}\text{H}_{42}\text{N}_{10}\text{Co}_2\text{O}_2$ requires C, 63.4; H, 4.62; N, 15.4 %;

Synthesis of $[\text{Co}_2(\text{OH})(\text{py})_2(\text{L}')][\text{Cl}]\cdot\text{CH}_2\text{Cl}_2$ – Under air, a solution of $\text{Co}(\text{OAc})_2\cdot 4\text{H}_2\text{O}$ (0.112 g, 0.447 mmol) in MeOH (4 mL) was added to a stirred suspension of $\text{H}_4\text{L}'$ (0.150 g, 0.213 mmol) in CH_2Cl_2 (15 mL) ($\text{H}_4\text{L}'$ is an analogue to H_4L that incorporates 2,3-naphthyl aromatic hinge groups derived from 2,3-naphthyldiamine). The resultant mixture was stirred for 20 minutes at room temperature, during which the solids had dissolved, and was treated with NEt_3 (ca. 0.2 mL). The dark brown solution was stirred at room temperature for 3.5 h, reduced in volume and 0.149 g, 82 % of crude $[\text{Co}_2(\text{O}_2)(\text{L}')]^+$ was precipitated by addition of Et_2O (20 mL). EPR (300K, CH_2Cl_2): g 2.027, $A(\text{Co})$ 10.31 G, $A(\text{N})$ 8.00 G; ESI-MS (+ve ion): m/z 835 ($[\text{Co}_2(\text{OH})(\text{L}')^+]^+$, 100 %). Black crystals of $[\text{Co}_2(\text{OH})(\text{py})_2(\text{L}')][\text{Cl}]\cdot\text{CH}_2\text{Cl}_2$ that were suitable for X-ray diffraction were obtained by diffusion of Et_2O into a CH_2Cl_2 /pyridine solution. The chloride has likely originated from the contamination of the bench CH_2Cl_2 solvent by HCl. Repeated efforts to obtain microanalytical data were unsuccessful, presumably as both hydroxide $[\text{Co}_2(\text{OH})(\text{py})_2(\text{L}')][\text{Cl}]$ and superoxocation $[\text{Co}_2(\text{O}_2)(\text{py})_2(\text{L}')^+]^+$ are present. ^1H NMR ($\text{CDCl}_3/\text{CD}_3\text{OD}$): δ_{H} 7.69 (t, 2 H, $J = 7.52$ Hz, pyridine), 7.58 (s, 4 H, imine), 7.38 (m, 4 H, pyridine), 7.32 (m, 4 H, aryl), 7.19 (m, 4 H, aryl), 7.12 (t, 4 H, $J_{\text{HH}} = 7.20$ Hz, pyridine), 7.08 (s, 4 H, aryl), 7.01 (d, 4 H, $J = 4.07$ Hz, pyrrole), 6.30 (d, 4 H, $J = 4.06$ Hz, pyrrole), 1.22 (s, 6 H, CH_3), 1.20 (s, 6 H, CH_3); ESI-MS (+ve ion): m/z 914 ($[\text{Co}_2(\text{OH})(\text{py})(\text{L}')^+]^+$, 20 %), 835 ($[\text{Co}_2(\text{OH})(\text{L}')^+]^+$, 100).

Catalytic measurements

(i) Rotating ring disk electrochemistry: RRD voltammograms were recorded in aqueous 1.0 M $\text{CF}_3\text{CO}_2\text{H}$ at 10 mVs^{-1} using a conventional three electrode cell comprising a Pine Instruments E6 series “ChangeDisk” rotating-ring-disk working electrode with a pyrolytic edge-plane-graphite (EPG) disk (area = 0.192 cm^2 , Le Carbone, Sussex, UK) and concentric platinum ring held at +1.0 V vs. AgCl/Ag, a platinum wire as the counter electrode and a AgCl/Ag reference electrode separated from the bulk by a salt bridge. The working electrode was rotated using a Pine Instruments AFMSRCE modulated speed rotator and experiments were controlled, and data recorded, by a PC-operated AFCBB1 bipotentiostat. Before use, the EPG disk was

polished separately to the Pt ring with 600 grit SiC paper, sonicated in distilled water for 1 min, and wiped dry. A solution of the catalyst (~ 0.1 mM) in THF was dropped on the surface of the disk and the solvent was allowed to evaporate.

(ii) Solution method: The reduction of dioxygen catalysed by $[\text{Co}_2(\text{L})]$ was studied in triplicate for three different catalyst concentrations using a modification of the procedures developed by Fukuzumi, Guilard, and co-workers.¹⁷ In a typical experiment, a solution of $[\text{Co}_2(\text{L})]$ (1.2×10^{-5} M) in anhydrous PhCN in the presence of an excess of Cp_2Fe (0.1 M) was transferred into a Teflon-tapped UV-Vis quartz cuvette under an inert atmosphere; a second aliquot of the same PhCN was then aerated and used to prepare a standard 0.02 M solution of $\text{CF}_3\text{CO}_2\text{H}$. A measured aliquot of this solution was then added to the UV cuvette such that the total concentration of O_2 (1.73 mM) was known. As soon as the solution of acid in PhCN was added (mixing was achieved by adding the acid by syringe to the bottom of the cuvette) the measurement was started and the concentration of ferrocenium produced was monitored at 620 nm ($\epsilon = 330 \text{ M}^{-1}\text{cm}^{-1}$) until asymptotic behaviour was observed. At the end of each hour long experiment, the solution was deaerated to inhibit any further reaction and treated with an excess of NaI. Diluted solutions were analysed by UV-vis spectrophotometry at 365 nm ($\epsilon = 28000 \text{ M}^{-1}\text{cm}^{-1}$) to quantify the I_3^- formed and so determine the amount of H_2O_2 present. Background oxidation of ferrocene by O_2 in the presence of acid under the same experimental conditions was subtracted from the data, and the quantity of H_2O_2 ($\sim 2 \times 10^{-5}$ M) determined by the above iodometric analysis. The function $\ln(A_\infty - A_t)$ was plotted versus time (for the first 100s) and the *pseudo*-first order rate constant k_{obs} was obtained as the slope of the graph for three different catalyst concentrations. Turnover frequency was calculated based on a 1000 s experiment.

[Cat], M	$[\text{Cp}_2\text{Fe}^+]$, M	$[\text{H}_2\text{O}_2]$, M	k_{obs} , s^{-1}	$[\text{H}_2\text{O}]$	% H_2O_2	TON H_2O	TOF H_2O , s^{-1}
1.2E-05	7.4E-04	2.6E-05	0.0079	1.7E-04	14.93	14.5	0.0145
1.2E-05	6.8E-04	7.8E-06	0.0057	1.7E-04	4.72	14.1	0.0141
1.2E-05	8.0E-04	1.3E-05	0.0050	1.9E-04	6.49	16.4	0.0164
1.8E-05	5.7E-04	8.6E-06	0.0084	1.4E-04	6.23	7.82	0.0078
1.8E-05	5.4E-04	8.5E-06	0.0077	1.3E-04	6.50	7.37	0.0074
1.8E-05	5.2E-04	8.5E-06	0.0080	1.3E-04	6.83	7.04	0.0070
2.4E-05	7.5E-04	2.4E-05	0.0056	1.8E-04	13.59	7.34	0.0073
2.4E-05	7.8E-04	1.4E-05	0.0056	1.9E-04	7.38	7.84	0.0078
2.4E-05	6.7E-04	1.2E-05	0.0059	1.6E-04	7.17	6.74	0.0067

Calculations - Restricted geometry optimisations were carried out for models of $[\text{Co}_2(\text{O}_2)(\text{py})_2(\text{L})]$ and $[\text{Co}_2(\text{O}_2)(\text{py})_2(\text{L})]^+$ using coordinates derived from the X-ray crystal structure of $[\text{Co}_2(\text{O}_2)(\text{py})_2(\text{L})]$. The electronic structures of the complexes were constrained to be low-spin during the geometry optimisations in line with the electronic structures determined from NMR and EPR experiments. The calculations were carried out using the Amsterdam Density Functional (ADF) suite version 2007.01.¹⁸ The DFT geometry optimisations

solution as two sets of *meso*-methyl group protons, assigned by integration, are observed at -26.1 and -30.4 ppm (the latter resonance overlaps coincidentally with a 4H resonance). Dark red crystals of $[\text{Co}_2(\text{L})]$ suitable for X-ray crystallography were grown from cold toluene, and the solid state structure is shown in Figure 1, with crystal data and selected bond lengths and angles detailed in Tables 1 and 2, respectively. Addition of pyridine to the crystallisation mixture results in the formation of dark red/black crystals of the pyridine adduct $[\text{Co}_2(\text{py})_2(\text{L})]$, the structure of which was described by us earlier,¹² and is shown in Figure 1 for comparison.

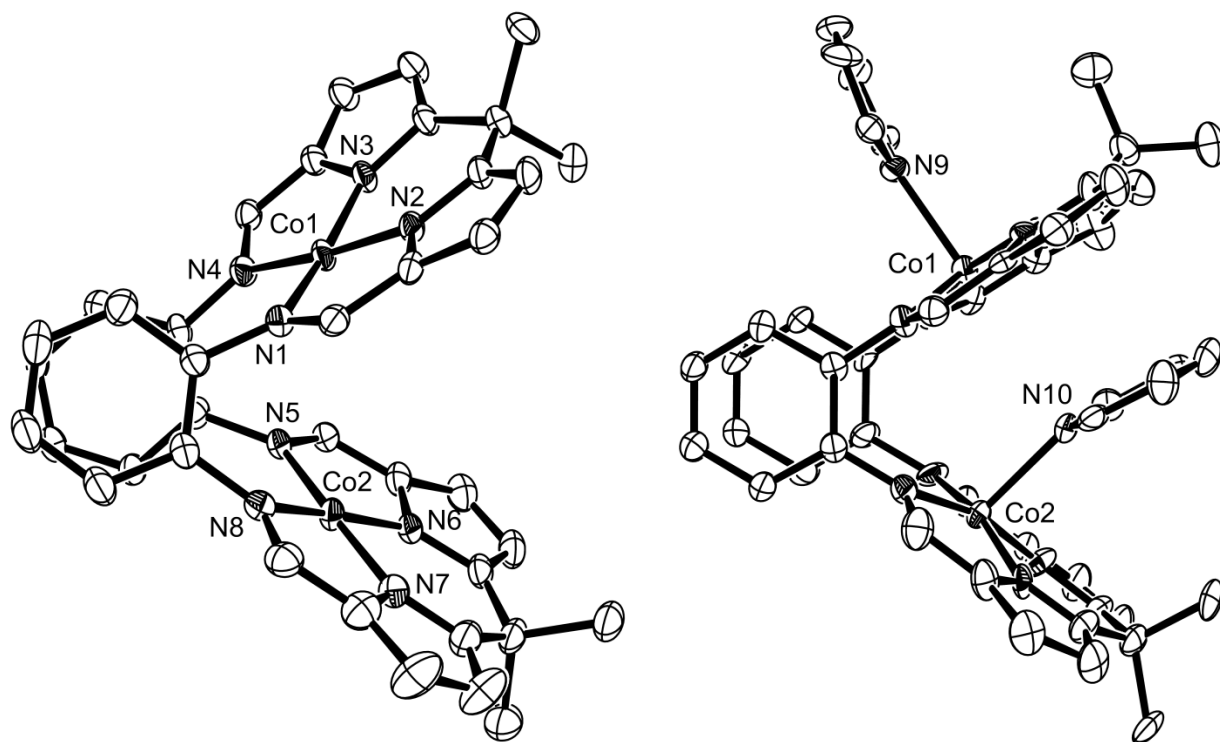


Figure 1. Solid state structures of $[\text{Co}_2(\text{L})]$ (left, one molecule from the asymmetric unit shown) and $[\text{Co}_2(\text{py})_2(\text{L})]$ (right) for comparison. For clarity, all hydrogen atoms and solvent molecules have been removed (50% probability displacement ellipsoids).

$[\text{Co}_2(\text{L})]$ crystallizes in the triclinic space group P-1, with two crystallographically-independent molecules in the unit cell; reference will be made to only one molecules as there are no significant differences between these two. As in solution, $[\text{Co}_2(\text{L})]$ adopts the wedged, or “Pacman” conformation in the solid state that has been seen before by us and others for many metal derivatives of this family of ligands. The two metals Co1 and Co2 sit in the centre of approximately square-planar N_4 -donor environments, in which the sum of the angles at Co1 is 359.95° and at Co2 is 360.13° , with out-of-plane distances 0.086 and 0.007 Å respectively. The two metal compartments are not cofacial, as the macrocycle adopts a skewed conformation defined by an average twist angle of 31.3° between the normal to the MN_4 plane and the plane(s) of the aromatic rings; this

skewed conformation is further reflected in the Co1•••Co2 separation of 4.12 Å. Although the metals sit in an approximately square planar environment, the *pseudo*-porphyrinic cavities are not entirely planar due to the flexibility of the N₄ donor set at the sp³ hybridised *meso*-carbon; this results in a dihedral angle between the N1-Co1-N2 and N3-Co1-N4 planes of 16.22°, with a smaller value found for the analogous distortion in the Co2 compartment (6.06°). Furthermore, the aromatic “hinges” diverge from coplanarity by 13.2°, although the interplanar distance of 3.438 Å (ring centroid - centroid) suggests the presence of significant π -stacking interactions.

Comparison of the structure of [Co₂(L)] to its doubly-solvated analogue (see Table 2 for geometric parameters) shows that both the average Co-N(imino) and Co-N(pyrrole) bond distances are longer in the latter, which is presumably a consequence of the expanded coordination sphere of the metal centre. Coordination of pyridine within the cleft also forces the macrocycle to adopt a more symmetric structure in which the twist angle in the pyridine adduct is decreased from 31.3° to 2.9°, the bite angle is increased from 62.6 to 64.8°, and the Co•••Co separation is elongated by 0.20 Å. In a similar manner to that seen by us in the binuclear copper complex [Cu₂(py)(L')], where L' is an analogous macrocycle derived from 2,3-diaminonaphthalene,¹⁰ the pyridine within the cleft adopts an unusually canted geometry in which the aromatic molecule π -stacks to the opposing N₄-plane, with an interplanar distance of 3.44 Å and dihedral angle of 3.3°, and hydrogen bonds to a suitably-oriented *meso*-methyl group (C_{meso}•••pyridine_{centroid} = 3.82 Å); this results in a Co2-N10-py_{centroid} angle of 162.3°. This is in contrast to binuclear cofacial diporphyrins that can accommodate solvents such as pyridine in more normal co-ordination modes within the cleft due to possibility of considerable vertical expansion,²³ a feature that generally necessitates the use of bulky N-donor ligands such as Bu^t-imidazole as axial bases to ensure no undesired *endo*-co-ordination of solvent occurs. This *endo*-co-ordination of small N-donor ligands by single-pillared diporphyrin complexes is exemplified in the X-ray crystal structures of the dicobalt bis(corrole) and the porphyrin-corrole complexes [Co(*exo*-py)Co(*endo*-py)(*exo*-py)(BCA)] and [Co(*exo*-py)(*endo*-py)(H₂PCX)], respectively, where BCA is an anthracyl-bridged, bis(corrole) ligand, and (H₂PCX) is a xanthyl-bridged porphyrin-corrole ligand in which the porphyrin cavity is unoccupied.²⁴ In both of these cases, one cobalt centre is octahedral with one of the axial pyridines bound within the binuclear cleft; even so, and unlike in [Co₂(*exo*-py)(*endo*-py)(L)], the wide ranging vertical expansion available to the porphyrinic ligand systems still results in near linear N(py)-Co-N(py) angles.

Synthesis and structures of dioxygen complexes [Co₂(O₂)(py)₂(L)] and [Co₂(O₂)(MeCN)₂(L)]

The dioxygen complexes [Co₂(O₂)(L)] and [Co₂(O₂)(py)₂(L)] can be synthesised by two methods: (i) by exposure of [Co₂(L)] to air; (ii) from the aerobic reaction of Co(OAc)₂ with H₄L under basic conditions. The former route is the more reproducible than the latter as it avoids problems that sometimes occur due to incomplete deprotonation of the macrocycle that can result in the formation of Co(II) acetate complexes such

as $[\text{HNEt}_3][\{\text{Co}_2(\text{OAc})(\mu\text{-OAc})(\text{H}_2\text{L})\}_2(\mu\text{-OAc})]\cdot\text{CH}_2\text{Cl}_2$ (see SI Figure S1 for X-ray crystal structure). In our previous communication,¹² the X-ray structure of $[\text{Co}_2(\text{O}_2)(\text{py})_2(\text{L})]$ was described, and showed that the dioxygen bridged the two Co centres within the macrocyclic cleft in a zigzag Pauling bonding mode (Figure 2). The O-O bond distance of 1.361(3) Å was found to be in-between the ranges reported for binuclear cobalt superoxo and peroxy complexes, and, furthermore, the Co-N and Co-O bond distances were not indicative of cobalt(II) or cobalt(III) oxidation states; as such, the degree of dioxygen reduction was not easily deduced from the crystallographic data. Instead, the use of ¹H NMR, EPR, and *in-situ* magnetic susceptibility experiments allowed us to identify the products of the oxygenation reaction as a mixture of the peroxy complex $[\text{Co}^{\text{III}}_2(\text{O}_2)(\text{py})_2(\text{L})]$ (90%) and the superoxo cation $[\text{Co}^{\text{III}}_2(\text{O}_2)(\text{py})_2(\text{L})]^+$ (10%). The lack of a counter ion such as chloride or hydroxide in the above solid state structure suggests that $[\text{Co}_2(\text{O}_2)(\text{py})_2(\text{L})]$ is indeed a peroxy-bridged complex. Attempts to oxidise the peroxy complex using standard oxidants such as I₂, either during an EPR experiment or as larger scale reactions, were unsuccessful. This suggests that the superoxo is not in equilibrium with the peroxy, but is instead generated as a result of oxidation of $[\text{Co}_2(\text{L})]^+$, which then reacts rapidly with more O₂ to form $[\text{Co}^{\text{III}}_2(\text{O}_2)(\text{py})_2(\text{L})]^+$. This rationale is consistent with that reported for analogous cofacial diporphyrin systems in which a single-electron reduction of a $[\text{Co}^{\text{III}}_2(\text{diporph})]^{2+}$ compound is required in order to promote O₂ binding and the formation of the superoxo complex $[\text{Co}_2(\text{O}_2)(\text{diporph})]^+$.

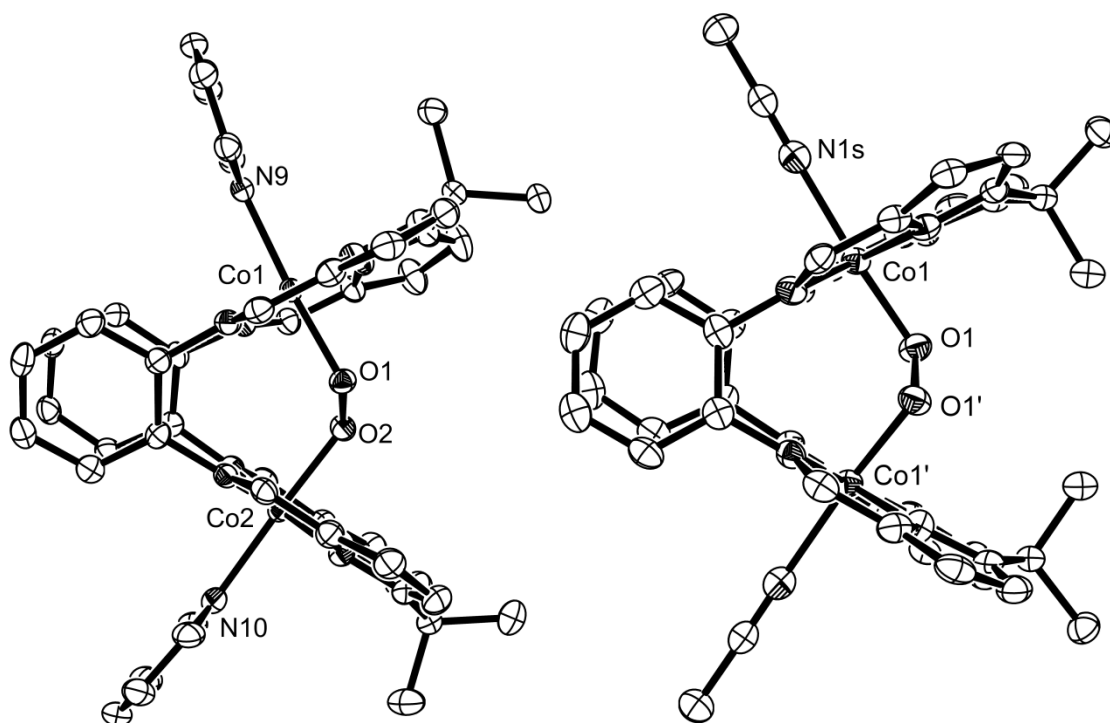


Figure 2. Solid state structures of the dioxygen complexes $[\text{Co}_2(\text{O}_2)(\text{py})_2(\text{L})]$ (left)¹² and $[\text{Co}_2(\text{O}_2)(\text{MeCN})_2(\text{L})]$ (right). For clarity, all hydrogens and solvent of crystallisation have been omitted (50% probability displacement ellipsoids); Co1' and O1' are the symmetry equivalents of Co1 and O1, respectively.

In an attempt to substantiate further the assignment of the Co oxidation states, XPS data were acquired on solid samples of $[\text{Co}_2(\text{L})]$, $[\text{Co}_2(\text{py})_2(\text{L})]$ and $[\text{Co}_2(\text{O}_2)(\text{L})]$. These data display an increase in the Co 2p binding energy moving from the Co(II) complexes $[\text{Co}_2(\text{L})]$ (Co 2p = 777.9 eV) and $[\text{Co}_2(\text{py})_2(\text{L})]$ (780.2) to the Co(III) oxygenated compound $[\text{Co}_2(\text{O}_2)(\text{L})]$ (780.8) that is consistent with an increase in metal oxidation state. Similarly, XPS studies of Co(salen) complexes and their dioxygen adducts reflect increased binding energies (*ca.* 1.0 eV) for the Co(III) compounds compared to the Co(II) precursors.²⁵ For these latter compounds, it was also shown that it is possible to differentiate between superoxo and peroxy through analysis of the O 1s binding energies, which vary by *ca.* 1.0 eV, but, unfortunately, in our case, we were unable to deconvolute the peroxy O 1s peak from background signals.

The sensitive nature of the binuclear complex $[\text{Co}_2(\text{L})]$ to aerobic oxidation was highlighted during attempts to crystallise it from cold (-30 °C) MeCN under N_2 , which resulted in the formation of dark red prisms; the X-ray crystal structure was determined (Figure 2) and crystal data are detailed in Table 1 and selected bond lengths and angles in Table 2. It is clear from these data that the crystal is a two component mixture comprising the binuclear cobalt(II) adduct $[\text{Co}_2(\text{MeCN})_2(\text{L})]$ and its oxygenated analogue $[\text{Co}_2(\text{O}_2)(\text{MeCN})_2(\text{L})]$; the data were refined satisfactorily with $wR_1 = 0.0745$ as a disordered merohedral twin with the dioxygen in 42% occupancy. Although the O1-O1' bond distance of 1.382(14) Å and other Co-ligand bond distances are not significantly different to that seen in the pyridine analogue $[\text{Co}_2(\text{O}_2)(\text{py})_2(\text{L})]$ (Table 2), a small change is seen in the cavity shape with both bite and twist angles, and the Co...Co separation decreased in the MeCN adduct. It is also clear the small and rigidly-constrained cleft size exhibited by this class of macrocyclic compound prohibits the linear binding of MeCN molecule within the cleft, and this contrasts to that seen by us in the binding of the planar pyridine guest in the adducts $[\text{Co}_2(\text{py})_2(\text{L})]$ and $[\text{Cu}_2(\text{py})(\text{L}^*)]$. Both $[\text{Co}_2(\text{O}_2)(\text{py})_2(\text{L})]$ and $[\text{Co}_2(\text{O}_2)(\text{MeCN})_2(\text{L})]$ exhibit extended structures in the solid state that are constructed from intermolecular C-H...O₂ short contacts between the cobalt-bound O₂ and pyridine or acetonitrile solvent CH bonds (see SI, Figures S2 and S3); in $[\text{Co}_2(\text{O}_2)(\text{py})_2(\text{L})]$, this results in a zigzag chain of molecules, while molecules of $[\text{Co}_2(\text{O}_2)(\text{MeCN})_2(\text{L})]$ form a square grid array. This interaction may indicate that the cobalt-bound O₂ possesses some Brønsted basicity, a feature that is desirable for promoting 4-electron over 2-electron dioxygen reduction chemistry (see below).¹³

Table 1. Crystal data^[a]

	[Co ₂ (L)]	[Co ₂ (O ₂)(MeCN) ₂ (L)]	[Co ₂ (OH)(py) ₂ (L)][Cl]
crystal size [mm]	1.30 × 0.20 × 0.04	0.01 × 0.01 × 0.01	0.30 × 0.18 × 0.15
crystal system	triclinic,	tetragonal,	monoclinic,
space group	<i>P</i> -1	<i>I</i> 4 ₁ / <i>a</i>	<i>P</i> 2 ₁ / <i>n</i>
temperature [K]	150 (2)	120 (2)	150 (2)
<i>a</i> , <i>b</i> , <i>c</i> [Å]	12.758(3), 13.278(3), 25.809(5)	13.140(5), 13.140(5), 41.905(9)	12.5220(8), 10.8201(7), 36.754(2)
α , β , γ [°]	87.028(3), 89.533(3), 68.176(3)	90.00, 90.00, 90.00	90.00, 93.692(1), 90.00
<i>V</i> [Å ³]	4053 (2)	7235 (4)	4969.4 (5)
<i>Z</i> , ρ [mg m ⁻³]	4, 1.404	8, 1.495	4, 1.489
radiation type, λ [Å]	Mo <i>K</i> α , 0.71073	Synchrotron, 0.6943	Mo <i>K</i> α , 0.71073
μ [mm ⁻¹]	0.87	0.97	0.88
$2\theta_{\max}$ [°]	55.0	46.28	54.9
diffractometer	Bruker SMART1000 CCD area detector	Bruker SMART APEX2 CCD diffractometer	Bruker SMART APEX CCD area detector
scan mode	ω	fine-slice ω scans	ω
absorption correction	multi-scan	multi-scan	multi-scan
<i>T</i> _{min} , <i>T</i> _{max}	0.354, 0.593	0.822, 1.000	0.779, 0.876
measured, independent reflns	35351, 18057	23109, 2604	42508, 11266
structure solution	direct methods using SHELXS	direct methods using SIR- 92	direct methods using SHELXS
structure refinement	full-matrix least squares using SHELXL	full-matrix least squares using SHELXL	full-matrix least squares using SHELXL
refinement on	<i>F</i> ²	<i>F</i> ²	<i>F</i> ²
θ_{\max} [°]	27.59	22.68	27.49
No. of parameters	1011	257	668
H-atom treatment	Riding model, rigid rotors for the Me groups	Riding model	Riding model
<i>R</i> [<i>F</i> ² > 2 σ (<i>F</i> ²)], <i>wR</i> (<i>F</i> ²)	0.0563, 0.130	0.035, 0.0745	0.0741, 0.1695
$\Delta\rho_{\max}$, $\Delta\rho_{\min}$ [e Å ⁻³]	0.97, -0.77	0.48, -0.34	1.944, -0.86
CSD numbers ^[b]	710017	710018	710019

[a] Computer programs: Bruker SMART version 5.624 (Bruker, **2001**); Bruker APEX2; Bruker SMART version 5.625 (Bruker, **2001**); SMART (Siemens, **1993**); Bruker SAINT version 6.36a (Bruker, **2002**); Bruker SAINT; Bruker SAINT version 6.36a (Bruker, **2000**); SAINT (Siemens, **1995**); Bruker SAINT; Bruker SHELXTL (Bruker, **2001**); SHELXS97 (Sheldrick, **1990**); Sir-92; SHELXS-97 (Sheldrick, **1990**); SIR-92 (Giacovazzo, **1994**); SHELXL97 (Sheldrick, **1997**); SHELXL-97 (Sheldrick, **1997**); ORTEP (Farrugia, **1997**); enCIFer (Allen et al., **2004**); PLATON (Spek, **2003**); enCIFer (Allen et al., **2004**). [b] CCDC 710017 - 710021 contain the supplementary crystallographic data for this paper. These data can be obtained free of charge from the Cambridge Crystallographic Data Centre vis www.ccdc.cam.ac.uk/data_request/cif.

Table 2. Comparison of key geometric parameters from X-ray and calculated data for the series of binuclear cobalt complexes of L (all distances (Å) and angles (°) are averaged unless singular). For definitions of bite and twist angles, see ref¹⁰

	[Co ₂ (L)]	[Co ₂ (py) ₂ (L)] Ref ¹²	[Co ₂ (O ₂)(py) ₂ (L)] Ref ¹²	[Co ₂ (O ₂)(py) ₂ (L)] (calculated)	[Co ₂ (O ₂)(py) ₂ (L)] ⁺ (calculated)	[Co ₂ (O ₂)(MeCN) ₂ (L)]	[Co ₂ (OH)(py) ₂ (L')] ⁺
Co-N(pyrrrole)	1.847	1.870	1.870	1.898	1.891	1.864	1.863
Co-N(imine)	1.949	1.974	1.984	2.044	2.052	1.998	1.988
Co-N(solv)	----	2.149	2.071	2.167	2.099	2.126	1.966
Co-O	----	----	1.934	1.942	1.891	1.891(7)	1.930
O-O	----	----	1.361(3)	1.336	1.334	1.382(14)	----
Co...Co	4.12	4.30	4.15	4.12	4.17	3.92	3.61
Bite	62.6	64.8	62.7	61.9	62.3	52.9	53.8
Twist	31.3	2.9	16.1	15.5	15.8	9.8	5.1
Co-O-O-Co	----	----	101.9	101.9	121.0	101.8	----
O/N-Co-N(solv)	----	----	175.6	173.7	176.0	161.1(2)	179.3

Dioxygen reduction catalysis

The significance of non-platinum metal catalysts for the reduction of dioxygen led us to evaluate the efficacy of [Co₂(L)] and its oxygenated products that are either generated *in situ* or as isolated compounds, as catalysts for this process. In the first instance, millimolar solutions of [Co₂(O₂)(L)]/[Co₂(O₂)(L)]⁺ were generated by dissolution of [Co₂(L)] in aerated CH₂Cl₂ and evaluated by cyclic voltammetry (CV).

The CV of [Co₂(L)] under air between +1.50 and -2.50 V in CH₂Cl₂ displays two irreversible oxidation waves at E_p^a +0.27 and +0.99 V and an associated weak reduction wave at E_p^c -0.19 V (Figure 3b). No further reduction waves were seen except for that due to O₂ reduction by the glassy carbon electrode at E_p^c -1.30 V (*cf.* Figure 3a, note: CF₃CO₂H absent). Scanning to high positive potential (> +0.99 V) resulted in the loss of electrochemical response due to coating of the working electrode. Closer inspection of the CVs between +0.39 and +0.05 V at varying scan rate gave a straight line fit for I_p^a vs. v^{0.5}, consistent with irreversibility of the oxidation at +0.27 V (SI, Figure S4), and CVs to more reducing voltages displayed related features at E_p^c +0.10, -0.13 and -0.22 V that are generated only after oxidation to +0.39 V, *i.e.* through an EC mechanism (Figure 3c). Significantly, by comparing the oxidation at +0.27 V to that of ferrocene added to the mixture (3.8 molar equivalents, SI Figure S5), it is clear that the oxidation at +0.27 V for [Co₂(O₂)(L)]/[Co₂(O₂)(L)]⁺ is

for less than one electron. Indeed, controlled potential electrolysis of a 4.6 μM sample of $[\text{Co}_2(\text{L})]$ under air at +0.36 V generated 58 mC of charge which equates to only 0.13 e^- . However, some insight is gained from these data, as we have shown previously that the reaction of $[\text{Co}_2(\text{L})]$ with air generates primarily the peroxy complex $[\text{Co}_2(\text{O}_2)(\text{L})]$ along with *ca.* 10 % of the superoxo cation $[\text{Co}_2(\text{O}_2)(\text{L})]^+$. It is therefore likely that the electrochemically-active species in this mixture is the latter superoxo cation, with the major peroxy product displaying no redox chemistry, and that the feature at +0.27 V represents a one electron irreversible oxidation to the unstable dication $[\text{Co}_2(\text{O}_2)(\text{L})]^{2+}$. Furthermore, the lack of any reductive redox processes shows that electrochemical interconversion of the superoxo cation and the peroxy complex does not occur and so they are presumably formed by different synthetic routes.

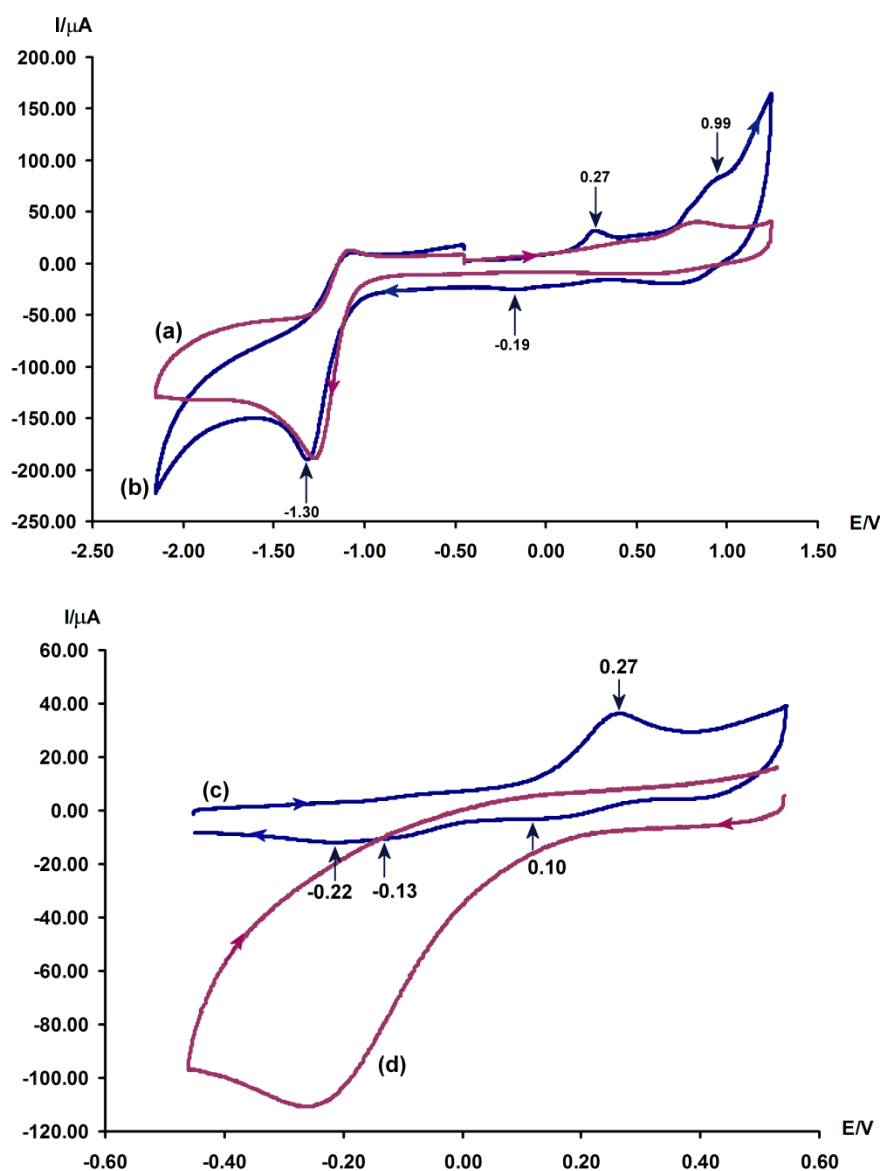


Figure 3. Assessment of $[\text{Co}_2(\text{L})]$ as an oxygen reduction catalyst by cyclic voltammetry under air: (a) no catalyst, (b) + $[\text{Co}_2(\text{L})]$, (c) + $[\text{Co}_2(\text{L})]$ range +0.55 to -0.45V, (d) + $\text{CF}_3\text{CO}_2\text{H}$. Conditions: 1.0 mM catalyst in

CH₂Cl₂, 0.4 M ⁿBu₄NBF₄ versus Fc⁺/Fc (AgCl/Ag reference electrode), glassy carbon working electrode (19.6 mm²), Pt wire counter electrode, scan rate 100 mVs⁻¹.

Addition of CF₃CO₂H to the electrochemical solution causes the feature at +0.27 V to disappear and a large reduction wave with E_p^c -0.27 V to evolve (Figure 3d); this feature is consistent with catalytic dioxygen reduction, and occurs at a potential *ca.* 0.5 V more positive than for glassy carbon alone (note: with no catalyst E_p^c = -0.76 V under same conditions); no reduction process is observed under a dinitrogen atmosphere. However, under these conditions this reduction wave is transient as sequential CVs between +0.55 and -0.45 V sees the height of the E_p^c peak diminish rapidly due to the working electrode becoming coated (SI Figure S6); re-polishing the electrode returns the electrochemical activity briefly before coating reoccurs.

In related cofacial diporphyrin chemistry, Le Mest, Saillard and co-workers have described the solution electrochemistry of a series of dicobalt cofacial and Pacman diporphyrin complexes in the presence of O₂.¹⁴ For example, for the Pacman complex [Co₂(DPA)], (where DPA is an anthracenyl-based single-pillared diporphyrin) they observed two oxidation processes at E_p^a 0.00 V and E_{1/2} +0.35 V (*vs.* Fc⁺/Fc) which were assigned to the formation of the hyperoxo complex [Co₂(O₂)(DPA)]⁺ (*i.e.* O₂³⁻) in which the O₂ unit was calculated to be side-on bound, and its single electron oxidation product [Co₂(O₂)(DPA)]²⁺, respectively; other diporphyrin complexes in this series behaved similarly. The hyperoxo complex [Co₂(O₂)(DPA)]⁺ was found to react with only one equivalent of acid to form the new π -radical [Co₂(O₂H)(DPA)]²⁺, which, on the addition of excess acid, resulted in a catalytic reduction wave at the reduction potential of [Co₂(O₂H)(diporph)]²⁺ (*ca.* 0.0 to -0.12 V). Similar electrochemical observations have been made by Nocera and co-workers for dicobalt complexes of 2nd generation Pacman ligands,^{6, 13} although in this case the resting state for the catalysis was the Co^{III}Co^{III} superoxo cation [Co₂(O₂)(diporph)]⁺ in which the O₂ unit was calculated to zigzag between the two metals (*i.e.* Pauling mode), and was generated by exposure of the cation [Co^{II}Co^{III}(diporph)]⁺ to air. These observations bear some similarity to those seen by us in the electrochemistry of oxygenated [Co₂(L)]. While, in our case, the superoxo complex is formed spontaneously on exposure of [Co₂(L)] to air, the further oxidation and catalytic reduction processes in the presence of acid are seen to occur at potentials similar to those of the cofacial diporphyrin complexes; as such, this suggests that the mechanism of catalytic dioxygen reduction by [Co₂(L)] is similar to that determined for cofacial diporphyrin analogues. In order to assess this reaction further, in particular to determine the relative proportions of H₂O₂ and H₂O produced, both solid state and solution electroreduction experiments were carried out.

Rotating Ring-Disk experiments were carried out using a standard Pine Instruments platinum ring and edge-plane-graphite (EPG) disk setup.^{8, 26} Typically, a drop of a [Co₂(L)] solution in THF was allowed to evaporate in air on the EPG electrode in order to ensure a homogeneous layer of active catalyst. The electrode was then

immersed in 1.0 M aqueous $\text{CF}_3\text{CO}_2\text{H}$ and a preliminary voltammetric scan was recorded between +800 and -800 mV versus Ag^+/Ag . An irreversible reduction wave at about +0.20 V was seen consistently, but as soon as the electrode was rotated, this wave lost intensity to eventually disappear after three voltammetric cycles, preventing the acquisition of a meaningful dataset and subsequent Koutecky-Levich analysis (Figure 4);²⁷ no ring current was detected in any experiments. It is therefore clear that the catalyst either does not adhere to the EPG disk or becomes inactive after a single cycle, as seen in the above CV experiments. Similar effects were observed during RRD electrochemical experiments of binuclear cofacial diporphyrins in which gradual catalyst deactivation occurred and necessitated recoating or complete repolishing and coating of the EPG disk.²⁸ In this case, it was thought that the catalyst became deactivated through chemical attack by superoxide or peroxide, rather than acid leaching of the chelated metal cation. In order to overcome a possible lack of adherence, attempts were made to graft the catalyst to the surface of the EPG electrode using mixtures of $[\text{Co}_2(\text{L})]$ and poly(vinylpyridine), Nafion, or methylcellulose. In each case, a similar reduction wave was observed initially that disappeared while regenerating the electrochemical diffusion layer for a new cycle, which suggests that a redox inactive complex is being formed during the catalytic cycle.

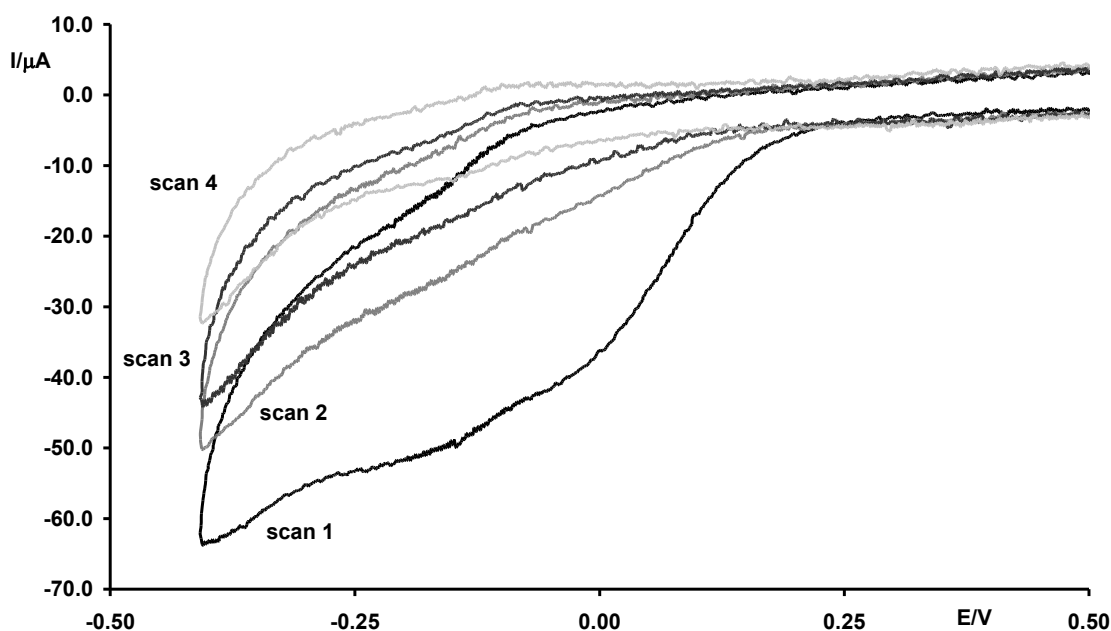


Figure 4. Sequential rotating ring disk electrochemistry of $[\text{Co}_2(\text{O}_2)(\text{L})]$ adsorbed on EPG disk in 1.0 M $\text{CF}_3\text{CO}_2\text{H}$ versus AgCl/Ag , rotation rate 500 rpm, Pt ring held at +1.0 V (ring efficiency 23%).

Fukuzumi, Guilard, and co-workers reported recently a solution method for determining the extent and products of catalytic dioxygen reduction using Cp_2Fe as the electron source in HClO_4 -acidified, air-saturated benzonitrile.¹⁷ In this method, the oxygen reduction reaction is assessed by monitoring the production of the

Cp_2Fe^+ cation at 620 nm by UV-vis spectrophotometry, and, from a simple determination of endpoint concentration of Cp_2Fe^+ , it is possible to identify the number of electrons involved in the process and gain mechanistic insight through rate analysis; by using *in-situ* UV-vis iodometric analysis, the quantity of peroxide can be determined. Using a similar procedure, we have found that $[\text{Co}_2(\text{L})]$ catalyses the PCET reduction reaction between Cp_2Fe , $\text{CF}_3\text{CO}_2\text{H}$, and O_2 in air-saturated benzonitrile, with the associated generation of Cp_2Fe^+ cation. The asymptotic behaviour of a representative experiment is displayed in Figure 5, plotted as $[\text{Cp}_2\text{Fe}^+]$ against time, with a representative calculation of k_{obs} inset.

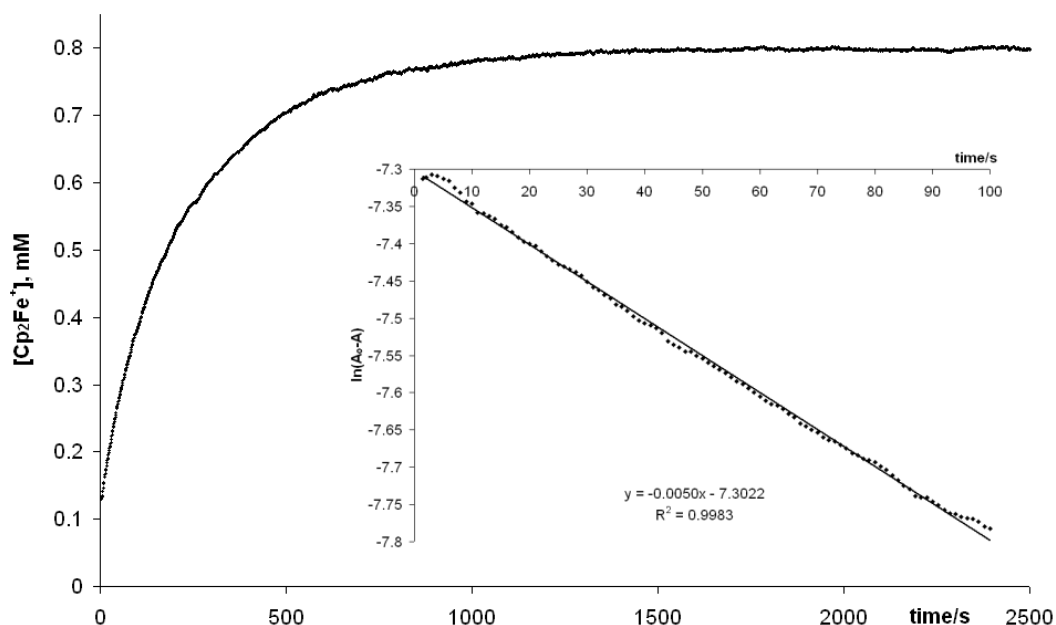


Figure 5. Typical experiment showing the evolution of $[\text{Cp}_2\text{Fe}^+]$ against time monitored by UV-vis spectrophotometry at 620 nm, catalyst concentration = 1.2×10^{-5} M, initial $[\text{Cp}_2\text{Fe}] = 0.1$ M, initial $[\text{CF}_3\text{CO}_2\text{H}] = 0.02$ M. Inset: calculation of k_{obs} as slope of the plot of $\ln(A_\infty - A)$ vs. time.

While it is clear from the ratio of endpoint concentration of Cp_2Fe^+ versus catalyst concentration (*ca.* 70:1) that the reaction is catalytic, not all the dioxygen is consumed; the ratio of $[\text{Cp}_2\text{Fe}^+]:[\text{O}_2]$ is *ca.* 0.4, and should be 2.0 for H_2O_2 production or 4.0 for H_2O production; as such, we are not able to determine the dioxygen reduction products from the concentration of Cp_2Fe^+ . However, *in-situ* analysis of the endpoint concentration of peroxide by addition of iodide to the reaction mixture and subsequent UV-visible spectroscopic determination of I_3^- provides some insight into the peroxide to water product ratio. The observed concentration of peroxide of between 7.8×10^{-6} and 2.4×10^{-5} M equates approximately to that determined from the background reaction between O_2 , Cp_2Fe , and $\text{CF}_3\text{CO}_2\text{H}$ (2×10^{-5} M after 1 h; see SI, Figure S7). This suggests that little or no peroxide is formed during the cobalt-catalysed reaction, and that therefore, in a similar manner to some of the porphyrinic analogues, the 4-electron reduction of O_2 to water is the predominant process. Even

so, it is clear that in our case the catalytically-active component diminishes over time as only 7-16 turnovers are achieved before the loss of activity. Furthermore, the rate of catalysis is very slow compared to cofacial diporphyrin analogues. Extrapolated values for the *pseudo*-first order rate constant k_{obs} average to $3.8(2) \times 10^{-3} \text{ s}^{-1}$, and are about three orders of magnitude smaller than the corresponding values obtained by Fukuzumi and co-workers using cofacial diporphyrins.¹⁷ In these latter cases, the reactions become asymptotic within minutes, while 30 to 60 min catalytic experiments are required in the case of $[\text{Co}_2(\text{L})]$.

Previous experimental and theoretical studies on related Co Pacman-diporphyrin complexes have found that the formation of a $\text{Co}^{\text{III}}/\text{Co}^{\text{III}}$ superoxo species from the reaction between a $\text{Co}^{\text{III}}/\text{Co}^{\text{II}}$ cation and O_2 is a critical entry point into the catalytic O_2 reduction cycle.^{13, 14, 29} Superoxo species have also been identified as a key component on platinum surfaces during oxygen reduction catalysis.³⁰ Also, in the porphyrinic systems, it has been determined that the basicity of the superoxo (or alternatively, the hyperoxo)¹⁴ complex dictates the mode of catalysis, in that initial protonation of the superoxo complex promotes a 4-electron reduction pathway to water, whereas rapid electron transfer first generates a transient peroxo complex which results in the 2-electron route being preferred.¹³ In our case, we can best consider that the *minor* (10 %) superoxo component of the Co material added represents the resting state of the catalytic cycle and that the peroxo compound (90 %) is effectively inert; this supposition would result in a ten-fold increase in TON. We noted above that we have been unable to isolate cleanly the superoxo compound $[\text{Co}_2(\text{O}_2)(\text{L})]^+$, either chemically or electrochemically, and that the peroxo and superoxo compounds are generated by different pathways. It is therefore feasible that the concentration of the catalytically-active species decreases during the reaction as diminishing amounts of superoxo complex are formed during the catalytic cycle, either as more peroxo compound and/or other inert compounds such as bridged hydroxides are produced (see below).

Mass spectrometry

Electrospray ionisation mass spectrometry and collision induced dissociation studies were used to explore the structure and fragmentation pathways of $[\text{Co}_2(\text{O}_2)(\text{L})]/[\text{Co}_2(\text{O}_2)(\text{L})]^+$ in the gas-phase. In previous electrospray ionisation studies on these complexes, we had not been able to stabilise the dioxygen compound, and instead the monoprotonated, single oxygen-containing species $[\text{Co}_2(\text{O})(\text{L})]\text{H}^+$ at m/z 735 that results from loss of O dominated the resulting mass spectrum.¹² In this study, by using an ion transfer tube temperature (the tube between atmospheric pressure and vacuum) of 63°C, a temperature considerably lower than is commonly applied in electrospray, the precursor ion $[\text{Co}_2(\mu\text{-O}_2)(\text{L})]\text{H}^+$ at m/z 751 was successfully detected and stabilised for the first time (Figure 6). Another ion at m/z 768 was also observed and is consistent with the presence of the hydroxyl adduct $[\text{OH}]\cdot[\text{Co}_2(\mu\text{-O}_2)(\text{L})]\text{H}^+$. Significantly, when the ion transfer tube temperature was increased, the single O-atom bridged species $[\text{Co}_2(\text{O})(\text{L})]\text{H}^+$ dominated the resulting mass spectrum, reflecting the labile nature of both $[\text{Co}_2(\mu\text{-O}_2)(\text{L})]\text{H}^+$ and its hydroxyl adduct $[\text{OH}]\cdot[\text{Co}_2(\mu\text{-O}_2)(\text{L})]\text{H}^+$.

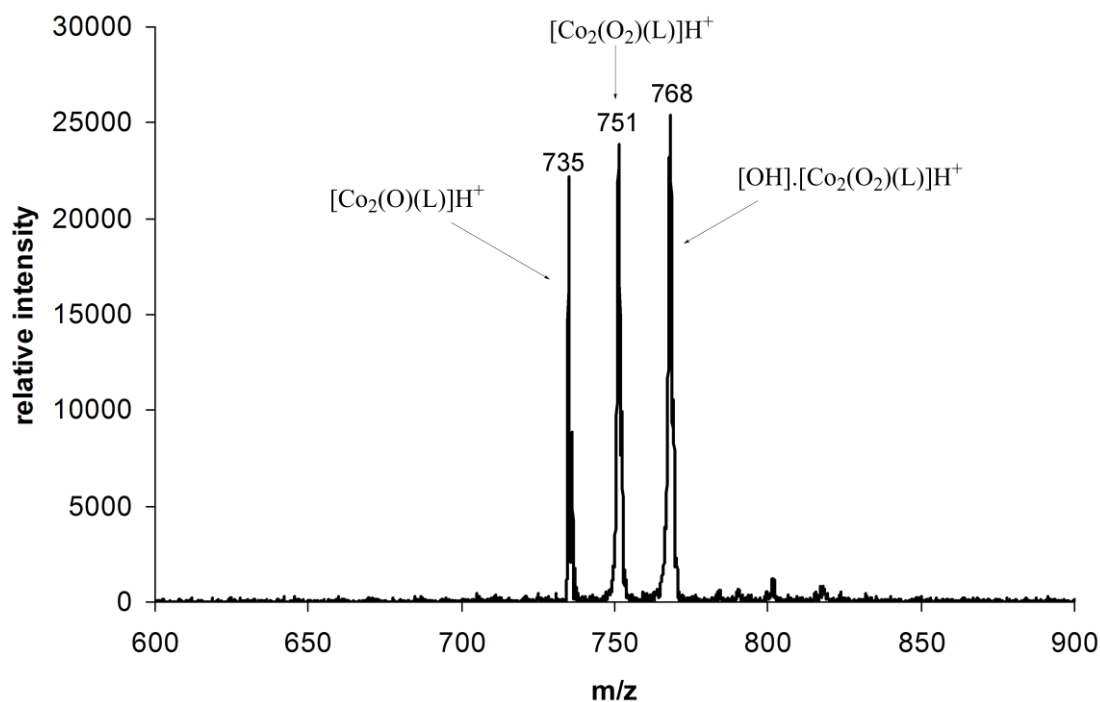


Figure 6. Typical ESI mass spectrum of $[\text{Co}_2(\text{O}_2)\text{L}]\text{H}^+$ obtained from a $18\mu\text{M}$ solution at low ion transfer capillary temperature (63°C).

In order to further investigate the stability and fragmentation pathways of $[\text{Co}_2(\text{O}_2)(\text{L})]\text{H}^+$ and its mono-oxygenated analogue $[\text{Co}_2(\text{O})(\text{L})]\text{H}^+$, collision induced dissociation (CID) studies were undertaken. CID is a popular tandem mass spectrometry method by which a particular ion type is activated through collisions with a buffer gas, in this case, helium.³¹ The detected products are a result of dissociation pathways including neutral ligand loss and hetero- and homolytic bond cleavage, as well as the possibility of charge transfer processes for multiply-charged ions. The quadrupole ion trap mass spectrometer used in this study enables the selective trapping and collisional-cooling of a mass-selected ion to produce a mass-normalised collision energy (NCE).³² As such, by recording CID spectra at increasing NCE, the extent of the activation of fragmentation pathways can be observed and used as a comparison of the relative stabilities of $[\text{Co}_2(\text{O})(\text{L})]\text{H}^+$ and $[\text{Co}_2(\text{O}_2)(\text{L})]\text{H}^+$ in the gas phase (Figure 7). It can be seen that higher collision energies are required to activate the fragmentation pathways of the single O-atom-bridged ion, $[\text{Co}_2(\text{O})(\text{L})]\text{H}^+$. Notably, for $[\text{Co}_2(\text{O}_2)(\text{L})]\text{H}^+$, the most facile loss is of a single oxygen atom whilst in the case of the mono-oxygenated species, a loss of a CH_3 group from the macrocyclic ligand is preferred. Indeed, we were not able to stabilise the deoxygenated ion $[\text{Co}_2(\text{L})]$ in this series of CID experiments, which suggests that the single O-atom bridged motif is particularly stable.

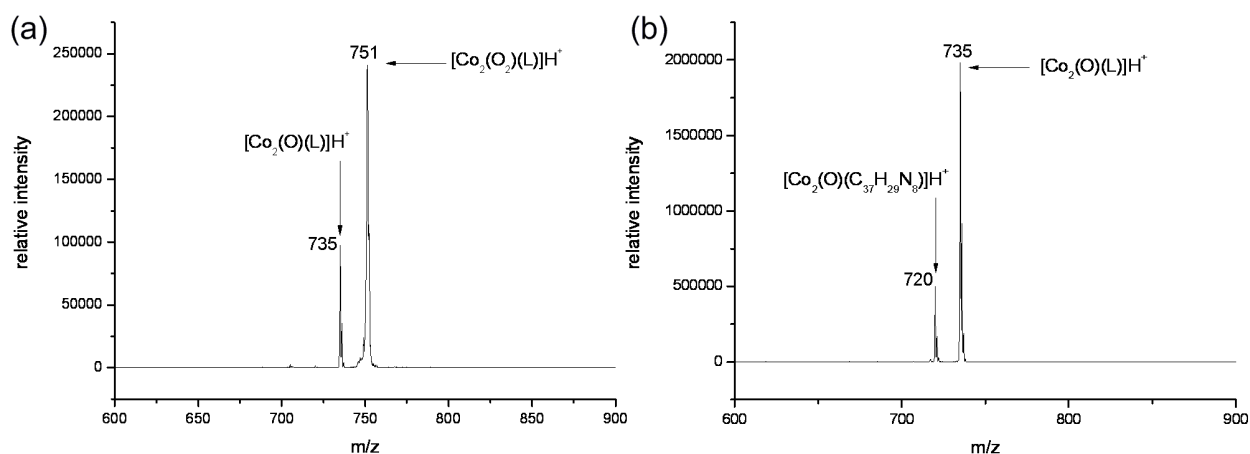


Figure 7. Collision induced dissociation spectra recorded for the precursor ions (a) $[\text{Co}_2(\text{O}_2)(\text{L})]\text{H}^+$ at 7% NCE; (b) $[\text{Co}_2(\text{O})(\text{L})]\text{H}^+$ 24% NCE.

Isolation and structural characterisation of single O-atom bridged complexes

Using a similar method to generate the dioxygen complex $[\text{Co}_2(\text{O}_2)(\text{py})_2(\text{L})]$, the aerobic reaction between $\text{Co}(\text{OAc})_2$ and $\text{H}_4\text{L}'$ under basic conditions ($\text{H}_4\text{L}'$ is an analogue to H_4L that incorporates 2,3-naphthyl aromatic hinge groups derived from 2,3-diaminonaphthalene) results in the formation of the new dicobalt complex $[\text{Co}_2(\mu\text{-OH})(\text{py})_2(\text{L}')][\text{Cl}]$ after recrystallisation from bench $\text{CH}_2\text{Cl}_2/\text{Et}_2\text{O}$ in the presence of pyridine. Analysis of the crude mixture by EPR spectroscopy revealed a very weak 15-line spectrum at $g = 2.027$ due to the presence of the superoxo cation $[\text{Co}_2(\text{O}_2)(\text{L}')]\text{H}^+$, so it is probable that this dioxygen complex has formed initially but is relatively unstable compared to the isolated hydroxy-bridged complex. The ^1H NMR spectrum of the crude mixture reveals resonances consistent with diamagnetic $[\text{Co}_2(\mu\text{-OH})(\text{py})_2(\text{L}')][\text{Cl}]$ and so supports the assignment of Co(III) oxidation states, and the presence of two resonances for the *meso*-methyl protons at 1.22 and 1.20 ppm implies that a wedged geometry is adopted in solution. Black crystals of $[\text{Co}_2(\mu\text{-OH})(\text{py})_2(\text{L}')][\text{Cl}]$ were obtained by diffusion of Et_2O into a mixture of CH_2Cl_2 and pyridine, and the solid state structure is shown in Figure 8 with crystal data and selected bond lengths and angles detailed in Tables 1 and 2, respectively.

The complex $[\text{Co}_2(\mu\text{-OH})(\text{py})_2(\text{L}')][\text{Cl}]$ crystallizes as a CH_2Cl_2 solvate in the monoclinic system, space group $P2_1/n$ and reveals the presence of a bridging oxygen atom within the cleft and a chloride counterion. The dichloromethane solvent of crystallisation contains a disordered chlorine atom Cl1 that was modelled over two sites with *ca.* 70:30 occupancy. The two Co atoms Co1 and Co2 sit in octahedral environments defined by the imino and two pyrrolic nitrogens, apical pyridines and the bridging oxygen atom. Even though the hydrogen was not located from the difference Fourier map, the latter oxygen is best defined as a bridging hydroxyl group rather than an oxo group due to a combination of the presence of the chloride counterion and

the diamagnetism of the complex. This is further substantiated by the average Co - O1 bond distance of 1.930 Å which are similar to other six-coordinate Co(III) bridging hydroxide complexes (mean 1.917 ± 0.036 Å).³³ The bridging hydroxide sits within the cleft of the macrocycle with a Co1-O1-Co2 angle of 138.4° that is considerably more obtuse than in reported examples (mean 102.0 ± 8.7 °),³³ and is presumably a consequence of the very rigid environment provided by the macrocycle. The presence of the hydroxyl bridge causes the bite angle of the Pacman wedge to decrease to 53.8° and limits the degree of torsional twisting in the solid state to 5.1° which results in a Co•••Co separation towards the lower limit of this series of compounds.

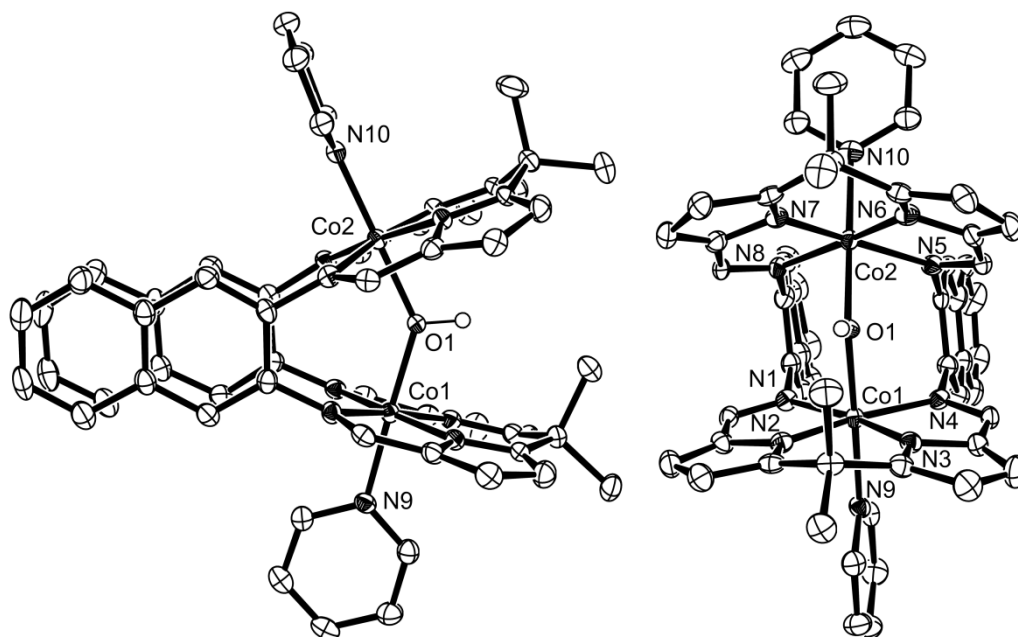


Figure 8. Side-on and face-on views of the solid state structure of $[\text{Co}_2(\text{OH})(\text{py})_2(\text{L}')][\text{Cl}]\cdot\text{CH}_2\text{Cl}_2$. For clarity, all hydrogen atoms except that on O1, chloride anion, and solvent of crystallisation have been omitted (50% probability displacement ellipsoids).

A second hydroxy-bridged dicobalt complex $[\text{Co}_2(\text{OH})(\text{Me}_2\text{Im})(\text{HL})](\text{MeCN})_4(\text{H}_2\text{O})$ crystallised in small quantities from acetonitrile during attempts to isolate $[\text{Co}_2(\text{L})]$ in the presence of 1, 2-dimethylimidazole (Me_2Im). The X-ray structure of this molecule (SI, Figure S8) showed that hydrolysis of a Co-N(pyrrole) bond had occurred to result in a $\text{Co}^{\text{II}}(\mu\text{-OH})\text{Co}^{\text{II}}$ motif in which one of the two five coordinate Co cations has migrated around the macrocycle to span the aryldiamine nitrogens. A similar bonding arrangement for the Co(II) cations is seen in $[\text{HNEt}_3][\{\text{Co}_2(\text{OAc})(\mu\text{-OAc})(\text{H}_2\text{L})\}_2(\mu\text{-OAc})]$ (see SI, Figure S1), although in contrast two pyrrole nitrogens remain protonated in this latter case. The Co-N and Co-O bond distances in $[\text{Co}_2(\text{OH})(\text{Me}_2\text{Im})_2(\text{HL})]$ suggest that Co(II) cations are present, as these distances are appreciable longer than those in the Co(III) complex $[\text{Co}_2(\text{OH})(\text{py})_2(\text{L}')]^+$. This is corroborated by comparison to $[\text{Co}_2(\mu\text{-OH})(\text{taec})][\text{ClO}_4]_3$ (taec = aminoethyl-substituted tetraazacyclotetradecane), a rare example of a structurally-characterised, singly-hydroxide-bridged binuclear Co(II) complex.³⁴

Calculations

The structural data from Amsterdam Density Functional calculations for $[\text{Co}_2(\text{O}_2)(\text{py})_2(\text{L})]$, $[\text{Co}_2(\text{O}_2)(\text{py})_2(\text{L})]^+$ and those derived from X-ray crystallographic studies are compared in Table 2. The calculated structure of $[\text{Co}_2(\text{O}_2)(\text{py})_2(\text{L})]$ reproduces the principal features of the structure of $[\text{Co}_2(\text{O}_2)(\text{py})_2(\text{L})]$ determined by X-ray crystallography, including the zig-zag $\kappa^1:\kappa^1$ Pauling bonding mode within the $[\text{Co}_2(\text{O}_2)]^{4+}$ unit and the bite and twist angles (bite = 61.9° and twist = 15.5°) between the macrocyclic components. The calculated metal-ligand distances are within 0.060 \AA of the experimental values, except for those involving the co-ordinated pyridine ligands which are *ca.* 0.096 \AA longer in the calculated structure. Thus, it is likely that the calculations reproduce qualitatively the principal features of the electronic structure of $[\text{Co}_2(\text{O}_2)(\text{py})_2(\text{L})]$. We also carried out calculations on $[\text{Co}_2(\text{O}_2)(\text{py})_2(\text{L})]^+$ since no experimental structure is available for this complex and because this species had been identified as a minor product (*ca.* 10%) in the reaction of $[\text{Co}_2(\text{L})]$ with O_2 . The superoxo complex $[\text{Co}_2(\text{O}_2)(\text{py})_2(\text{L})]^+$ possesses a similar electronic structure to peroxo $[\text{Co}_2(\text{O}_2)(\text{py})_2(\text{L})]$ in which the composition of the SOMO of $[\text{Co}_2(\text{O}_2)(\text{py})_2(\text{L})]^+$ (Figure 9b) is essentially identical to that of $[\text{Co}_2(\text{O}_2)(\text{py})_2(\text{L})]$ and is derived from the removal of one electron from the HOMO of $[\text{Co}_2(\text{O}_2)(\text{py})_2(\text{L})]$ (Figure 9a). The compositions of the SOMO in $[\text{Co}_2(\text{O}_2)(\text{py})_2(\text{L})]^+$ and HOMO in $[\text{Co}_2(\text{O}_2)(\text{py})_2(\text{L})]$ are 40.2% O 2p and 32.1% Co 3d, and 39.6% O 2p and 45.0% Co 3d, respectively.

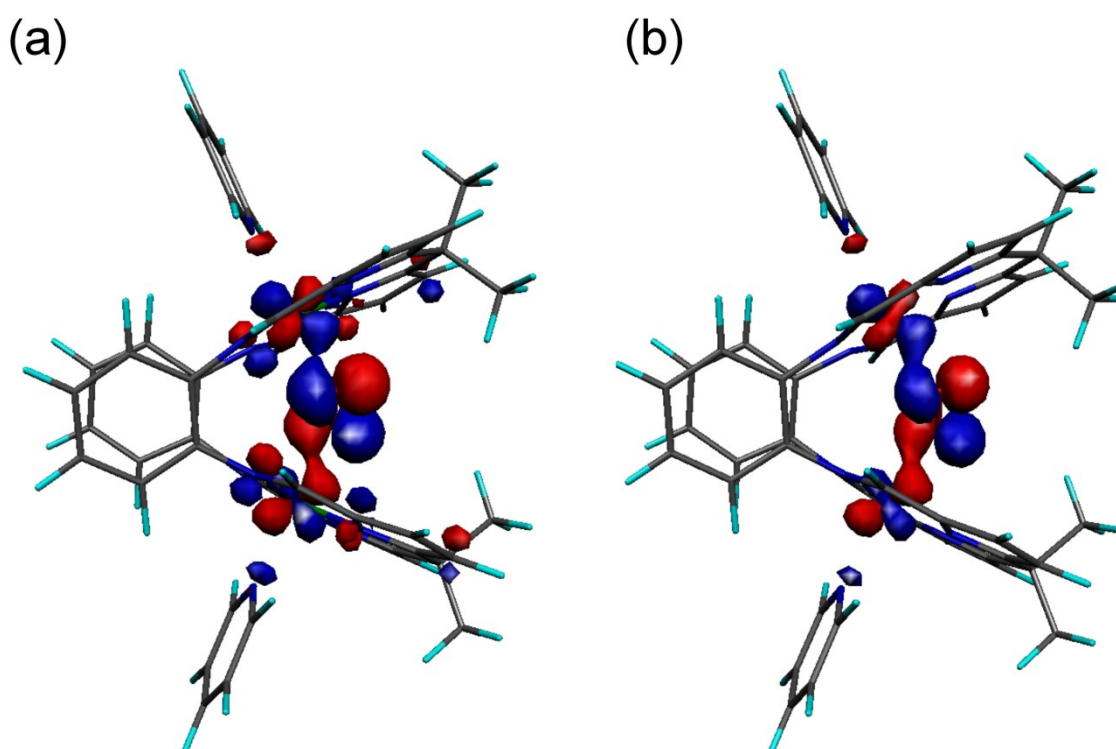


Figure 9. The Kohn-Sham representations of (a) the HOMO in $[\text{Co}_2(\text{O}_2)(\text{py})_2(\text{L})]$ and (b) the SOMO of $[\text{Co}_2(\text{O}_2)(\text{py})_2(\text{L})]^+$ at the 0.04 e\AA^{-3} isosurface (The program MOLEKEL³⁵ was used to prepare the three-dimensional plots of the electron density).

The calculated structure of $[\text{Co}_2(\text{O}_2)(\text{py})_2(\text{L})]^+$ retains the principal features of the co-ordination spheres about each metal found in $[\text{Co}_2(\text{O}_2)(\text{py})_2(\text{L})]$, with no significant variation in the Co-N (pyrrole and imine) and Co-O distances. $[\text{Co}_2(\text{O}_2)(\text{py})_2(\text{L})]^+$ possesses similar bite and twist angles (bite = 62.3° and twist = 15.8°) to those found for the calculated structure of $[\text{Co}_2(\text{O}_2)(\text{py})_2(\text{L})]$ (Table 2). The principal differences in geometry between $[\text{Co}_2(\text{O}_2)(\text{py})_2(\text{L})]$ and $[\text{Co}_2(\text{O}_2)(\text{py})_2(\text{L})]^+$ lie within the $[\text{Co}_2(\text{py})_2(\text{O}_2)]^{3+}$ unit. For $[\text{Co}_2(\text{O}_2)(\text{py})_2(\text{L})]^+$ the Co-N(py) and Co-O distances shorten by 0.094 \AA and 0.043 \AA , respectively, and the Co-O-O-Co dihedral angle increases from 101.9° in $[\text{Co}_2(\text{O}_2)(\text{py})_2(\text{L})]$ to 121.0° in $[\text{Co}_2(\text{O}_2)(\text{py})_2(\text{L})]^+$. Significantly however, the O-O distance is effectively unchanged on oxidation, decreasing very slightly from 1.336 \AA in $[\text{Co}_2(\text{O}_2)(\text{py})_2(\text{L})]$ to 1.334 \AA in $[\text{Co}_2(\text{O}_2)(\text{py})_2(\text{L})]^+$, and suggests that this bond distance is not a good measure of the formal electronic structure of these macrocyclic complexes and that the macrocyclic framework acts as a geometric constraint. In order to gain insight into the relative stabilities of the $[\text{Co}_2(\text{O}_2)(\text{py})_2(\text{L})]$ and $[\text{Co}_2(\text{O}_2)(\text{py})_2(\text{L})]^+$ complexes, we computed the reduction potential of the $[\text{Co}_2(\text{O}_2)(\text{py})_2(\text{L})]^{+/0}$ couple in CH_2Cl_2 solution and evaluated the molecular energies for the oxidized and reduced species in the same solvent:³⁶

$$V = -[(E_{red} - E_{ox}) + (\Delta G_{red}^{\text{CH}_2\text{Cl}_2} - \Delta G_{ox}^{\text{CH}_2\text{Cl}_2})] - V_0$$

where E_x and $\Delta G_x^{\text{CH}_2\text{Cl}_2}$ are the theoretical molecular and solvation energies, respectively and V_0 is the absolute potential (4.43 V)³⁷ of the normal hydrogen electrode (NHE). Using this methodology we calculate a reduction potential of $+0.37 \text{ V vs. NHE}$ for the $[\text{Co}_2(\text{O}_2)(\text{py})_2(\text{L})]^{+/0}$ couple ($-0.18 \text{ V vs. Fe}^+/\text{Fe}$); as such, the calculations suggest that the peroxo species $[\text{Co}_2(\text{O}_2)(\text{py})_2(\text{L})]$ is more thermodynamically stable than the superoxo cation $[\text{Co}_2(\text{O}_2)(\text{py})_2(\text{L})]^+$ in dichloromethane solution. This potential, together with the lack of electrochemical interconversion seen above between the peroxo and superoxo complexes, and the possible formation of very stable hydroxy-bridged motifs to form compounds such as $[\text{Co}_2(\mu\text{-OH})(\text{L}')^+]^+$, may inhibit access to the catalytically-relevant superoxo $[\text{Co}_2(\text{O}_2)(\text{py})_2(\text{L})]^+$ complex and depress the activity of these complexes towards oxygen reduction catalysis.

Conclusions

We have shown that a variety of dicobalt Pacman complexes of straightforwardly-synthesised Schiff-base calixpyrrole ligands can be prepared, and that their structures and chemistry related to oxygen reduction display some similarity to those of cofacial diporphyrins. The dicobalt complex $[\text{Co}_2(\text{L})]$ reacts readily with O_2 to form not only the peroxo complex $[\text{Co}_2(\text{O}_2)(\text{L})]$ but also the superoxo cation $[\text{Co}_2(\text{O}_2)(\text{L})]^+$ as a minor component. This mixture acts as a catalyst for the reduction of oxygen to water, albeit at low turnover number and frequency. As with the related cofacial diporphyrin chemistry, our present understanding based on electrochemical, mass spectrometric, catalytic, and DFT experiments is that the superoxo cation $[\text{Co}_2(\text{O}_2)(\text{L})]^+$ is the catalytically-relevant species, yet is disfavoured when compared to peroxo $[\text{Co}_2(\text{O}_2)(\text{L})]$ and hydroxy-

bridged species $[\text{Co}_2(\text{OH})(\text{L})]^+$. It is therefore clear that while this bimetallic structural motif can manage the proton and electron inventories necessary to carry out this reduction chemistry, modifications are required to inhibit the formation of peroxy and single-atom bridged complexes and to promote the formation of the superoxo cation $[\text{Co}_2(\text{O}_2)(\text{L})]^+$.

References:

- [1] Adler, S. B., *Chem. Rev.* **2004**, 104, 4791; Lewis, N. S.; Nocera, D. G., *Proc. Nat. Acad. Sci. USA* **2006**, 103, 15729; Dempsey, J. L.; Esswein, A. J.; Manke, D. R.; Rosenthal, J.; Soper, J. D.; Nocera, D. G., *Inorg. Chem.* **2005**, 44, 6879.
- [2] Alonso-Vante, N.; Feng, Y., *Phys. Stat. Sol. (B)*, **2008**, 245, 1792; Matter, P. H.; Biddinger, E. J.; Ozkan, U. S., *Catalysis* **2007**, 20, 338; Wang, B., *J. Power Sources* **2005**, 152, 1.
- [3] Bezerra, C. W. B.; Zhang, L.; Lee, K.; Liu, H.; Marques, A. L. B.; Marques, E. P.; Wang, H.; Zhang, J., *Electrochim. Acta* **2008**, 53, (15), 4937.
- [4] Bashyam, R.; Zelenay, P., *Nature* **2006**, 443, 63.
- [5] Rosenthal, J.; Nocera, D. G., *Prog. Inorg. Chem.* **2007**, 55, 483; Collman, J. P.; Wagenknecht, P. S.; Hutchinson, J. E., *Angew. Chem. Int. Ed.* **1994**, 33, 1537.
- [6] Rosenthal, J.; Nocera, D. G., *Acc. Chem. Res* **2007**, 40, 543.
- [7] Kadish, K. M.; Shen, J.; Fremond, L.; Chen, P.; El Ojaimi, M.; Chkounda, M.; Gros, C. P.; Barbe, J.-M.; Ohkubo, K.; Fukuzumi, S.; Guillard, R., *Inorg. Chem.* **2008**, 47, (15), 6726; Kadish, K. M.; Fremond, L.; Burdet, F.; Barbe, J.-M.; Gros, C. P.; Guillard, R., *J. Inorg. Biochem.* **2006**, 100, (4), 858; Kadish, K. M.; Shao, J.; Ou, Z.; Fremond, L.; Zhan, R.; Burdet, F.; Barbe, J.-M.; Gros, C. P.; Guillard, R., *Inorg. Chem.* **2005**, 44, (19), 6744; Rosenthal, J.; Chng, L. L.; Fried, S. D.; Nocera, D. G., *Chem. Commun.* **2007**, (25), 2642; Soper, J. D.; Kryatov, S. V.; Rybak-Akimova, E. V.; Nocera, D. G., *J. Am. Chem. Soc.* **2007**, 129, (16), 5069; Liu, S.-Y.; Nocera, D. G., *J. Am. Chem. Soc.* **2005**, 127, 5278; Chng, L. L.; Chang, C. J.; Nocera, D. G., *Org. Lett.* **2003**, 5, (14), 2421; Yeh, C.-Y.; Chang, C. J.; Nocera, D. G., *J. Am. Chem. Soc.* **2001**, 123, (7), 1513.
- [8] Kadish, K. M.; Fremond, L.; Ou, Z.; Shao, J.; Shi, C.; Anson, F. C.; Burdet, F.; Gros, C. P.; Barbe, J.-M.; Guillard, R., *J. Am. Chem. Soc.* **2005**, 127, (15), 5625.
- [9] Givaja, G.; Blake, A. J.; Wilson, C.; Schröder, M.; Love, J. B., *Chem. Commun.* **2003**, 2508; Arnold, P. L.; Patel, D.; Blake, A. J.; Wilson, C.; Love, J. B., *J. Am. Chem. Soc.* **2006**, 128, 9610; Arnold, P. L.; Patel, D.; Wilson, C.; Love, J. B., *Nature* **2008**, 451, 315; Volpe, M.; Reid, S. D.; Blake, A. J.; Wilson, C.; Love, J. B., *Inorg. Chim. Acta.* **2007**, 360, 273.
- [10] Givaja, G.; Volpe, M.; Leeland, J. W.; Edwards, M. A.; Young, T. K.; Darby, S. B.; Reid, S. D.; Blake, A. J.; Wilson, C.; Wolowska, J.; McInnes, E. J. L.; Schröder, M.; Love, J. B., *Chem. Eur. J.* **2007**, 13, 3707.

- [11] Cuesta, L.; Tomat, E.; Lynch, V. M.; Sessler, J. L., *Chem. Commun.* **2008**, (32), 3744; Veauthier, J. M.; Tomat, E.; Lynch, V. M.; Sessler, J. L.; Mirsaidov, U.; Markert, J. T., *Inorg. Chem.* **2005**, 44, 6736; Sessler, J. L.; Tomat, E.; Mody, T. D.; Lynch, V. M.; Veauthier, J. M.; Mirsaidov, U.; Markert, J. T., *Inorg. Chem.* **2005**, 44, (7), 2125; Sessler, J. L.; Cho, W.-S.; Dudek, S. P.; Hicks, L.; Lynch, V. M.; Huggins, M. T., *J. Porphyrins Phthalocyanines* **2003**, 7, 97; Veauthier, J. M.; Cho, W.-S.; Lynch, V. M.; Sessler, J. L., *Inorg. Chem.* **2004**, 43, 1220.
- [12] Givaja, G.; Volpe, M.; Edwards, M. A.; Blake, A. J.; Wilson, C.; Schröder, M.; Love, J. B., *Angew. Chem. Int. Ed.* **2007**, 46, 584.
- [13] Chang, C. J.; Loh, Z.-H.; Shi, C.; Anson, F. C.; Nocera, D. G., *J. Am. Chem. Soc.* **2004**, 126, 10013.
- [14] Le Mest, Y.; Inisan, C.; Laouenan, A.; L'Her, M.; Talarmin, J.; El Khalifa, M.; Saillard, J.-Y., *J. Am. Chem. Soc.* **1997**, 119, (26), 6095.
- [15] Burger, H.; Wannagat, U., *Monatsh. Chem.* **1963**, 94, 1007.
- [16] Schubert, E. M., *J. Chem. Educ.* **1992**, 69, 62; Evans, D. F., *J. Chem. Soc.* **1959**, 2003.
- [17] Fukuzumi, S.; Okamoto, K.; Gros, C. P.; Guillard, R., *J. Am. Chem. Soc.* **2004**, 126, (33), 10441.
- [18] Fonseca Guerra, C.; Snijders, J. G.; te Velde, G.; Baerends, E. J., *Theor. Chem. Acc.* **1998**, 99, 391; Velde, G. T.; Bickelhaupt, F. M.; Baerends, E. J.; Guerra, C. F.; Van Gisbergen, S. J. A.; Snijders, J. G.; Ziegler, T., *J. Comput. Chem.* **2001**, 22, 931.
- [19] Vosko, S. H.; Wilk, L.; Nusair, M., *Can. J. Phys.* **1980**, 58, 1200.
- [20] Becke, A. D., *Phys. Rev. A* **1988**, 38, 3098.
- [21] Perdew, J. P., *Physical Review B* **1986**, 33, 8822.
- [22] Klamt, A., *J. Phys. Chem.* **1995**, 2224; Klamt, A.; Jones, V., *J. Chem. Phys.* **1996**, 9972; Klamt, A.; Schüürmann, G., *J. Chem. Soc., Perkin Trans* **1993**, 799.
- [23] Deng, Y.; Chang, C. J.; Nocera, D. G., *J. Am. Chem. Soc.* **2000**, 122, 410.
- [24] Barbe, J.-M.; Burdet, F.; Espinosa, E.; Guillard, R., *Eur. J. Inorg. Chem.* **2005**, 1032; Guillard, R.; Jerome, F.; Barbe, J.-M.; Gros, C. P.; Ou, Z.; Shao, J.; Fischer, J.; Weiss, R.; Kadish, K. M., *Inorg. Chem.* **2001**, 40, (19), 4856.
- [25] Burness, J. H.; Dillard, J. G.; Taylor, L. T., *J. Am. Chem. Soc.* **1975**, 97, 6080; Lauher, J. W.; Lester, J. E., *Inorg. Chem.* **1973**, 12, 244.

- [26] Melin, F.; Boudon, C.; Lo, M.; Schenk, K. J.; Bonin, M.; Ochsenbein, P.; Gross, M.; Weiss, J., *J. Porphyrins Phthalocyanines* **2007**, 11, (3-4), 212.
- [27] Chen, J.; Zhang, W.; Officer, D.; Swiegers, G. F.; Wallace, G. G., *Chem. Commun.* **2007**, 3353; Treimer, S.; Tang, A.; Johnson, D. C., *Electroanalysis* **2002**, 14, 165.
- [28] Collman, J. P.; Denisevich, P.; Konai, Y.; Marrocco, M.; Koval, C.; Anson, F. C., *J. Am. Chem. Soc.* **1980**, 102, 6027.
- [29] Collman, J. P.; Hutchison, J. E.; Angel Lopez, M.; Tabard, A.; Guilard, R.; Seok, W. K.; Ibers, J. A.; L'Her, M., *J. Am. Chem. Soc.* **1992**, 114, 9869; Chang, C. K., *J. Chem. Soc., Chem. Commun.* **1977**, 800; Proniewicz, L. M.; Odo, J.; Goral, J.; Chang, C. K.; Nakamoto, K., *J. Am. Chem. Soc.* **1989**, 111, 2105.
- [30] Shao, M.-H.; Liu, P.; Adzic, R. R., *J. Am. Chem. Soc.* **2006**, 128, 7408.
- [31] March, R. E.; Todd, J. F. J., *Quadrupole Ion trap Mass Spectrometry*. 2nd ed.; Wiley Interscience: 2005; p 120.
- [32] Thermo-Scientific *Normalised Collision Energy Technology*; Product Support Bulletin 4; www.thermo.com/ms.
- [33] Fletcher, D. A.; McMeeking, R. F.; Parkin, D., *J. Chem. Inf. Comput. Sci.* **1996**, 36, 746.
- [34] Mikuriya, M.; Kida, S.; Kohzuma, T.; Murase, I., *Bull. Chem. Soc. Jpn* **1988**, 61, 2666.
- [35] Portmann, S.; Luthi, H. P., *Chimia* **2000**, 54, 766.
- [36] Fu, Y.; Liu, L.; Yu, H.-Z.; Wang, Y.-M.; Guo, Q.-X., *J. Am. Chem. Soc.* **2005**, 127, 7227.
- [37] Reiss, H.; Heller, A., *J. Phys. Chem.* **1985**, 89, 4207.